Central exclusive diffractive production of a single photon in high-energy proton-proton collisions within the tensor-Pomeron approach

Piotr Lebiedowicz [1,*] Otto Nachtmann,[2,†] and Antoni Szczurek[1,‡,§]

[1]*Institute of Nuclear Physics Polish Academy of Sciences, Radzikowskiego 152, PL-31342 Kraków, Poland*
[2]*Institut für Theoretische Physik, Universität Heidelberg,
Philosophenweg 16, D-69120 Heidelberg, Germany*

We discuss central-exclusive production (CEP) of photons via different fusion processes in the reaction $pp \to pp\gamma$ at high energies, available at RHIC and LHC, within the tensor-Pomeron model. We consider two types of processes, the photoproduction contribution via the photon-Pomeron and photon-Reggeon fusion reactions, and the purely diffractive contribution via the Reggeon-Pomeron and Odderon-Pomeron fusion reactions. We present predictions for the measurements of photons at midrapidity, $|y| < 2.5$, and at relatively low transverse momentum, $0.1 \text{ GeV} < k_\perp < 1 \text{ GeV}$. To check the main results of our study the measurement of the outgoing protons is not necessary. This is of relevance, e.g., for the present version of the ALICE detector at the LHC. Several differential distributions, for instance, in y, $k_\perp$, and ω, the rapidity, the absolute value of the transverse momentum, and the energy of the photon, respectively, are presented. We show that the photoproduction is an important process in the kinematic region specified above. There it gives a much larger cross section than diffractive bremsstrahlung where the basic $pp \to pp$ reaction is due to strong interaction diffraction. This is remarkable as the CEP cross section is of order α_{em}^3 whereas the bremsstrahlung one is only of order α_{em}. On the other hand, the soft-photon bremsstrahlung is more important than CEP in the forward rapidity range, $|y| > 4$, and/or at very low $k_\perp$. We leave it as a challenge for the planned ALICE 3 experiment at the LHC to study these two contributions to soft photon production in pp collisions. This could shed new light on the so-called "soft photon puzzle" in hadron-hadron collisions.

I. INTRODUCTION

In this article we continue our investigations of exclusive photon production in high-energy hadronic collisions in the tensor-Pomeron approach. In [1] we have treated $\pi\pi$ scattering without and with photon radiation. In [2] we have discussed the soft-photon bremsstrahlung in the $pp \to pp\gamma$ reaction. In the present paper we extend our considerations to central-exclusive production (CEP) processes of single photon in high-energy proton-proton collisions.

The $pp \to pp\gamma$ reaction was not yet measured at high energies. There is, however, a plan for a new multipurpose

---
*Piotr.Lebiedowicz@ifj.edu.pl
†O.Nachtmann@thphys.uni-heidelberg.de
‡Antoni.Szczurek@ifj.edu.pl
§Also at College of Natural Sciences, Institute of Physics, University of Rzeszów, ul. Pigonia 1, PL-35310 Rzeszów, Poland.

detector at the LHC, ALICE 3 [3–6], that would be able to measure ultrasoft photons at very low transverse momentum in pp, pA, and AA collisions. The main aim of our paper is to discuss CEP processes in the exclusive $pp \to pp\gamma$ reaction at low transverse momentum of the photon for the LHC energy range.

A measurement of the soft-photon production at the LHC could shed light on a long-standing discrepancy between the theoretical predictions of the bremsstrahlung, based on Low's theorem [7], and the measured soft-photon spectra in several hadronic reactions. For experiments on soft photon production see Refs. [8–19]. Overviews of the experimental and theoretical status of this "soft photon puzzle" are given in [4,20]. The question is if there is production of so called "anomalous soft photons," and if so, what is the origin of these photons. From our point of view the origin of such anomalous terms should be searched for in nonperturbative QCD processes. In this paper we will consider a conventional source of "anomalous photons," that is, photons from CEP reactions. For unconventional sources of anomalous photons see, e.g., Refs. [21,22] and the review in [20].

In order to calculate the cross section for $pp \to pp\gamma$ we use the tensor-Pomeron and vector-Odderon model

proposed in [23]. In this model, the charge-conjugation $C = +1$ exchanges, that is, the Pomeron $\mathbb{P}$ and the Reggeons $\mathbb{R}_+ = f_{2\mathbb{R}}, a_{2\mathbb{R}}$ are treated as effective rank-2 symmetric tensor exchanges, the $C = -1$ Odderon $\mathbb{O}$ and the Reggeons $\mathbb{R}_- = \omega_{\mathbb{R}}, \rho_{\mathbb{R}}$ are described as effective vector exchanges. In [24] the helicity structure of high-energy pp elastic scattering at small momentum transfers was calculated. It was shown there that the STAR data [25] exclude a scalar character of the Pomeron-proton coupling but are perfectly compatible with the tensor-Pomeron model. The assumption of a vector character for the Pomeron couplings has theoretical and experimental problems as discussed in [24,26]. In [26] it was shown that for a Pomeron coupling to photons like a vector its contribution to real Compton scattering and hence to the total γp photoabsorption cross section vanishes exactly. A further result of [26] is that a vector Pomeron cannot contribute to the forward virtual Compton amplitude which leads to the conclusion of its decoupling in the structure functions of low-x deep inelastic scattering (DIS). On the other hand, the data for the total γp photoabsorption cross section and the low-x structure functions clearly indicate that at high energies Pomeron exchange must be present as a *main* contribution. And indeed, in the tensor-Pomeron model a very satisfactory fit of these data was obtained; see Ref. [26]. Applications of the tensor-Pomeron concept were given for photoproduction of pion pairs in [27] and for a number of diffractive CEP reactions in pp collisions at high energies [28–39].

Several processes contribute to the $pp \to pp\gamma$ reaction. One of them is CEP of single photons through the $\gamma - \mathbb{P}$-fusion process. In order to calculate the relevant amplitudes we need the $\mathbb{P}\gamma\gamma$ coupling functions. In addition to the $\gamma - \mathbb{P}$-fusion process we shall also estimate the subleading $\gamma - f_{2\mathbb{R}}$-fusion process. The *Ansätze* for the relevant vertices for real and virtual photons are discussed in [23,26,40]. The Q^2 and t dependencies of the coupling functions in the Pomeron/Reggeon-photon-photon vertices must be determined from a comparison to experimental data. We shall use the parametrizations obtained in [40] from a comparison of the tensor-Pomeron model to the elastic γp-scattering data from FNAL and to the deeply virtual Compton scattering (DVCS) data measured at HERA. The CEP of photons via the $\gamma - \mathbb{P}$-fusion process can be expected to populate preferentially the midrapidity region as was discussed earlier in [41] within another approach. In the present paper, we shall also discuss CEP of single photons through the $\mathbb{R}_- - \mathbb{P}$, $\mathbb{R}_- - \mathbb{R}_+$, $\mathbb{O} - \mathbb{P}$, and $\mathbb{O} - \mathbb{R}_+$ fusion processes within the tensor-Pomeron and vector-Odderon approach [23]. We wish to estimate the size of the cross sections for these processes for the LHC energy range. In a first approximation we neglect absorption effects due to the proton-proton interactions.

Our paper is organized as follows. In the next section we give analytic expressions for the amplitudes for the $pp \to pp\gamma$ reaction. Different CEP fusion processes such as $\gamma - \mathbb{P}$, $\rho_{\mathbb{R}} - \mathbb{P}$, and $\mathbb{O} - \mathbb{P}$ are discussed. The results of our calculations are presented in Sec. III. Section IV contains a summary and our conclusions. In Appendix A we list the expressions for the effective propagators and vertices used in our model. Appendix B is devoted to an approximate calculation of $pp \to pp\gamma$ using the method of the equivalent photon spectrum. This gives us an understanding of the size of the cross sections obtained with our model. In Appendix C we discuss the CEP mechanism for photons in the soft photon limit $k \to 0$, where k is the photon's four-momentum.

II. THEORETICAL FORMALISM

We consider the reaction

$$p(p_a, \lambda_a) + p(p_b, \lambda_b)$$
$$\to p(p_1', \lambda_1) + p(p_2', \lambda_2) + \gamma(k, \epsilon). \quad (2.1)$$

The momenta are indicated in brackets, the helicities of the protons are denoted by $\lambda_a, \lambda_b, \lambda_1, \lambda_2 \in \{1/2, -1/2\}$, and ϵ is the polarization vector of the photon.

The kinematic variables are

$$s = (p_a + p_b)^2 = (p_1' + p_2' + k)^2,$$
$$q_1 = p_a - p_1', \qquad t_1 = q_1^2,$$
$$q_2 = p_b - p_2', \qquad t_2 = q_2^2,$$
$$s_1 = W_1^2 = (p_1' + k)^2 = (p_a + q_2)^2,$$
$$s_2 = W_2^2 = (p_2' + k)^2 = (p_b + q_1)^2,$$
$$u_1 = (p_a - p_2')^2, \qquad u_2 = (p_b - p_1')^2. \quad (2.2)$$

In the overall c.m. system we choose the 3 axis in the direction of $\boldsymbol{p_a}$. The rapidity of the photon is then

$$\mathrm{y} = \frac{1}{2} \ln \frac{k^0 + k^3}{k^0 - k^3} = -\ln \tan \frac{\theta}{2}, \quad (2.3)$$

where θ is the polar angle of $\boldsymbol{k}$, $k^3 = |\boldsymbol{k}| \cos \theta$. Furthermore, $\omega = k^0$ is the energy of the photon, $\omega = |\boldsymbol{k_\perp}| \cosh \mathrm{y}$.

The $\mathcal{T}$-matrix element for the reaction (2.1) is

$$\langle p(p_1', \lambda_1), p(p_2', \lambda_2), \gamma(k, \epsilon) | \mathcal{T} | p(p_a, \lambda_a), p(p_b, \lambda_b) \rangle$$
$$= (\epsilon^\mu)^* \mathcal{M}_\mu^{(\text{total})}(p_a, \lambda_a; p_b, \lambda_b; p_1', \lambda_1; p_2', \lambda_2; k). \quad (2.4)$$

The amplitude must be antisymmetric under interchange of the two final protons

$$\mathcal{M}_\mu^{(\text{total})}(p_a, \lambda_a; p_b, \lambda_b; p_1', \lambda_1; p_2', \lambda_2; k)$$
$$= -\mathcal{M}_\mu^{(\text{total})}(p_a, \lambda_a; p_b, \lambda_b; p_2', \lambda_2; p_1', \lambda_1; k) \quad (2.5)$$

and gauge invariance requires

$$k^\mu \mathcal{M}_\mu^{(\text{total})} = 0. \tag{2.6}$$

We are interested in high c.m. energies $\sqrt{s}$ and small momentum transfers $|t_1|, |t_2|$:

$$\sqrt{s} \gg m_p, \qquad |t_1|, |t_2| \lesssim c m_p^2, \qquad c = \mathcal{O}(1). \tag{2.7}$$

In this kinematic region the amplitude (2.4) is governed by t-channel exchanges. Let us denote the corresponding amplitude by

$$\mathcal{M}_\mu^{(t\text{-channel})}(p_a, \lambda_a; p_b, \lambda_b; p_1', \lambda_1; p_2', \lambda_2; k). \tag{2.8}$$

With the exchange of the final-state protons we get the u-channel exchange amplitude,

$$\mathcal{M}_\mu^{(u\text{-channel})} = \mathcal{M}_\mu^{(t\text{-channel})}\big|_{(p_1', \lambda_1) \leftrightarrow (p_2', \lambda_2)}. \tag{2.9}$$

The total amplitude for (2.1) is then

$$\mathcal{M}_\mu^{(\text{total})} = \mathcal{M}_\mu^{(t\text{-channel})} - \mathcal{M}_\mu^{(u\text{-channel})}. \tag{2.10}$$

In the kinematic region (2.7) the u-channel-exchange term on the right-hand side (rhs) of (2.10) is expected to give negligible contribution. Therefore, in the following we omit the term $\mathcal{M}_\mu^{(u\text{-channel})}$ in our considerations and, for brevity of notation, we set

$$\mathcal{M}_\mu \equiv \mathcal{M}_\mu^{(t\text{-channel})}. \tag{2.11}$$

As discussed in Sec. II C of Ref. [2] the cross section for the photon yield can then be calculated as follows

$$d\sigma(pp \to pp\gamma)$$
$$= \frac{1}{2\sqrt{s(s - 4m_p^2)}} \frac{d^3 k}{(2\pi)^3 2k^0} \int \frac{d^3 p_1'}{(2\pi)^3 2p_1'^0} \frac{d^3 p_2'}{(2\pi)^3 2p_2'^0}$$
$$\times (2\pi)^4 \delta^{(4)}(p_1' + p_2' + k - p_a - p_b)$$
$$\times \frac{1}{4} \sum_{p \text{ spins}} \mathcal{M}_\mu \mathcal{M}_\nu^*(-g^{\mu\nu}); \tag{2.12}$$

see Eq. (2.35) of Ref. [2].

In the calculations we can consider the amplitude $\mathcal{M}_\mu$ (2.11) as a sum due to the bremsstrahlung (BS) and the CEP processes contributing to $pp \to pp\gamma$[1]:

---

[1]In the general case a strict separation of bremsstrahlungs and CEP contributions is not possible; see the discussion in Appendix C.

$$\mathcal{M}_\mu = \mathcal{M}_\mu^{(\text{BS})} + \mathcal{M}_\mu^{(\text{CEP})}. \tag{2.13}$$

The amplitude $\mathcal{M}_\mu^{(\text{BS})}$ corresponds to diffractive bremsstrahlung discussed in [2]; see the diagrams (a)–(f) of Fig. 3 there. In this mechanism, the amplitudes corresponding to photon emission from the external protons are determined by the off-shell pp elastic scattering amplitude and the contact terms needed in order to satisfy gauge-invariance constraints. For details how to calculate the bremsstrahlung contribution in our approach we refer the reader to Sec. II and Appendix B of Ref. [2].

The amplitude for central-exclusive production (CEP) of photons is given by the sum of the contributions from the relevant fusion processes

$$\mathcal{M}_\mu^{(\text{CEP})} = \mathcal{M}_\mu^{(\gamma - \mathbb{P})} + \mathcal{M}_\mu^{(\gamma - \mathbb{R}_+)} + \mathcal{M}_\mu^{(\mathbb{R}_- - \mathbb{P})} + \mathcal{M}_\mu^{(\mathbb{R}_- - \mathbb{R}_+)}$$
$$+ \mathcal{M}_\mu^{(\mathbb{O} - \mathbb{P})} + \mathcal{M}_\mu^{(\mathbb{O} - \mathbb{R}_+)}. \tag{2.14}$$

Here, $\mathbb{R}_+$ denotes the $C = +1$ Reggeons ($f_{2\mathbb{R}}, a_{2\mathbb{R}}$), and $\mathbb{R}_-$ denotes the $C = -1$ Reggeons ($\omega_\mathbb{R}, \rho_\mathbb{R}$). Different fusion processes should be considered, these involving the photon, $\gamma - \mathbb{P}$ and $\gamma - \mathbb{R}_+$, as well as purely diffractive contributions $\mathbb{R}_- - \mathbb{P}$, $\mathbb{R}_- - \mathbb{R}_+$, $\mathbb{O} - \mathbb{P}$, and $\mathbb{O} - \mathbb{R}_+$. In fact, we consider the exchange of soft ($\mathbb{P}_1$) and hard ($\mathbb{P}_0$) Pomeron. Thus, $\mathbb{P}$ in (2.14) stands for the sum of $\mathbb{P}_1$ and $\mathbb{P}_0$, $\mathbb{R}_+$ for $f_{2\mathbb{R}}$ and $a_{2\mathbb{R}}$, and $\mathbb{R}_-$ for $\omega_\mathbb{R}$ and $\rho_\mathbb{R}$.

It is interesting to list the leading order in $e = \sqrt{4\pi\alpha_{\text{em}}}$ with which the various processes contribute to $\mathcal{M}_\mu$; see Table I. Thus, naively one could expect that the fusion processes $\gamma - \mathbb{P}$ and $\gamma - \mathbb{R}_+$ give small contributions since they are of higher order in e, compared e.g. to diffractive bremsstrahlung. But, as we shall see, in certain regions of phase space these e^3 processes are the dominant ones.

In the following, we will discuss the CEP contributions (2.14) in detail.

A. Photoproduction contributions

First we consider the fusion processes involving photon exchange, $\gamma - \mathbb{P}$ and $\gamma - \mathbb{R}_+$. The corresponding diagrams are shown in Fig. 1. We have for the $\gamma - \mathbb{P}$ contribution in Eq. (2.14)

TABLE I. The leading order in e of the various processes contributing to $pp \to pp\gamma$; see (2.13) and (2.14). By diffractive and QED bremsstrahlung we denote the processes where the basic $pp \to pp$ reaction is due to strong interaction diffraction and exchange of a photon, respectively.

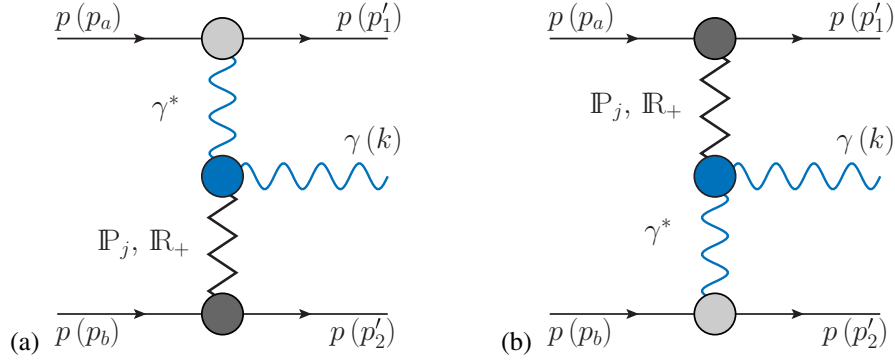| Process	Leading order in e
Diffractive bremsstrahlung	e
QED bremsstrahlung	e^3
Fusion $\gamma - \mathbb{P}$, $\gamma - \mathbb{R}_+$	e^3
Fusion $\mathbb{O} - \mathbb{P}$, $\mathbb{O} - \mathbb{R}_+$, $\mathbb{R}_- - \mathbb{P}$, $\mathbb{R}_- - \mathbb{R}_+$	e

FIG. 1. Diagrams for CEP of a photon in high-energy proton-proton collisions: (a) photon-Pomeron/Reggeon fusion; (b) Pomeron/Reggeon-photon fusion. We have $j = 0, 1$ with $\mathbb{P}_0$ and $\mathbb{P}_1$ denoting the hard and soft Pomeron, respectively, and $\mathbb{R}_+$ stands for the sum of $f_{2\mathbb{R}}$ and $a_{2\mathbb{R}}$ Reggeons.

$$\mathcal{M}_\mu^{(\gamma-\mathbb{P})} = \mathcal{M}_\mu^{(\gamma\mathbb{P})} + \mathcal{M}_\mu^{(\mathbb{P}\gamma)}. \qquad (2.15)$$

Here and in the following we indicate by $(\gamma\mathbb{P})$ the amplitude obtained from to the diagram Fig. 1(a) and by $(\mathbb{P}\gamma)$ that obtained from Fig. 1(b). The sum of these two amplitudes is indicated by $(\gamma - \mathbb{P})$. For other CEP processes we use the analogous notation.

The lower part of the diagram in Fig. 1(a) corresponds exactly to the DVCS diagram for $\gamma^* p \to \gamma p$ at a reasonably high c.m. energy W_2 such that the t-channel exchanges dominate. In [40] we have studied this reaction in the tensor-Pomeron-approach and we obtained a good description of the data for large c.m. energies and small Bjorken x values. This is the kinematic region where our model should be valid. How can we assure for the reaction (2.1), which we study in the present paper, that we are in a kinematic region where our model is valid? Let us consider first the diagram of Fig. 1(a). In the lower part of the diagram, the DVCS part, we should thus have high enough energy, $W_2 \gtrsim 6$ GeV say, and small Bjorken x corresponding to $|t_1|/W_2^2 \ll 1$. For the diagram of Fig. 1(b) the analogous conditions are $W_1 \gtrsim 6$ GeV and $|t_2|/W_1^2 \ll 1$. However, imposing such conditions by hand would be inconvenient from an experimental point of view, since it would require the measurement of the final state protons. Instead we shall only impose conditions on the photon kinematics. We shall require the photon transverse momentum $k_\perp$ to be in the range 0.1 GeV $< k_\perp <$ 1 GeV and we shall require large rapidity gaps between the centrally produced photon and the outgoing protons, that is, we require for the photon rapidity $|y| < 2.5$. The large rapidity gaps will assure dominance of Pomeron exchange in the diagrams of Fig. 1. We shall see below in Sec. III that, indeed, these requirements assure that we can safely use the diagrams of Fig. 1 for the calculation of the amplitudes for (2.1).

Some comments are in order here. If we consider instead of CEP of a photon the CEP of a meson M of mass m_M the situation is quite different. Let us, for instance, consider the production of the meson M at rest in the overall c.m. system. We have then automatically large subenergies squared $W_1^2, W_2^2 \approx m_M \sqrt{s}$ and the exchange diagrams analogous to Figs. 1(a) and 1(b) should be valid representations of the amplitude. This argument clearly fails for the massless photon. But, as we shall see in Sec. III, considering CEP of the photon at midrapidity region and at low transverse momentum already ensures large enough energies $W_{1,2}$. Finally we note that we could extend our calculation of CEP of $\gamma(k)$ with γ^* exchange to a larger region of phase space using representations of the DVCS data valid for higher values of Bjorken x and smaller energies $W_{1,2}$. For some remarks on this problem see Appendix C. But a complete discussion of such an extended calculation goes beyond the scope of our present paper.

Now we come back to the calculation of the diagrams of Fig. 1. We consider there the exchanges of $\mathbb{P}_1$, $\mathbb{P}_0$, and $\mathbb{R}_+$ that correspond to the soft Pomeron, the hard Pomeron, and the Reggeons $(f_{2\mathbb{R}} + a_{2\mathbb{R}})$, respectively. The *Ansätze* for effective propagator and vertex functions of these exchanges are taken from [23,26] and are discussed in Appendix A. In the tensor Pomeron model the Pomeron- and Reggeon-$\gamma\gamma$ vertices have two coupling functions; see (A5). By comparing the tensor-Pomeron model and the experimental data on real Compton scattering from FNAL and on DVCS obtained by the H1 and ZEUS Collaborations at HERA we fixed in [40] these coupling functions. In our calculations we shall use the FIT 2 parametrization from [40] [see (A10) in Appendix A].

The $\gamma\mathbb{P}$-exchange amplitude can now be written as

$$\mathcal{M}_\mu^{(\gamma\mathbb{P})} = (-i)\sum_{j=0,1}\bar{u}(p'_1,\lambda_1)i\Gamma_{\nu_1}^{(\gamma pp)}(p'_1,p_a)u(p_a,\lambda_a)i\Delta^{(\gamma)\nu_1\nu}(q_1)i\Gamma_{\mu\nu\kappa\rho}^{(\mathbb{P}_j\gamma^*\gamma^*)}(k,q_1)$$

$$\times\, i\Delta^{(\mathbb{P}_j)\kappa\rho,\alpha\beta}(s_2,t_2)\bar{u}(p'_2,\lambda_2)i\Gamma_{\alpha\beta}^{(\mathbb{P}_j pp)}(p'_2,p_b)u(p_b,\lambda_b)$$

$$= i\sum_{j=0,1}\bar{u}(p'_1,\lambda_1)\Gamma^{(\gamma pp)\nu}(p'_1,p_a)u(p_a,\lambda_a)\frac{1}{t_1}\frac{1}{2s_2}(-is_2\alpha'_{\mathbb{P}_j})^{\alpha_{\mathbb{P}_j}(t_2)-1}$$

$$\times\,[2a_{\mathbb{P}_j\gamma^*\gamma^*}(t_1,k^2,t_2)\Gamma_{\mu\nu}^{(0)\alpha\beta}(k,-q_1) - b_{\mathbb{P}_j\gamma^*\gamma^*}(t_1,k^2,t_2)\Gamma_{\mu\nu}^{(2)\alpha\beta}(k,-q_1)]\bar{u}(p'_2,\lambda_2)\Gamma_{\alpha\beta}^{(\mathbb{P}_j pp)}(p'_2,p_b)u(p_b,\lambda_b). \quad (2.16)$$

We use the standard γ propagator and the γpp vertex, see (3.1) and (3.26)–(3.32) of Ref. [23], respectively. All effective propagator and vertex functions for the $\mathbb{P}_j$ exchanges used in (2.16) are listed in Appendix A.

For the $\mathbb{P}\gamma$-exchange amplitude [see Fig. 1(b)] we have the same structure as for the amplitude (2.16) with the replacements

$$(p(p_a,\lambda_a),p(p'_1,\lambda_1)) \leftrightarrow (p(p_b,\lambda_b),p(p'_2,\lambda_2)),$$

$$t_1 \leftrightarrow t_2, \quad q_1 \leftrightarrow q_2, \quad s_2 \leftrightarrow s_1. \quad (2.17)$$

In a similar way we obtain the $\gamma\mathbb{R}_+$- and $\mathbb{R}_+\gamma$-exchange amplitudes.

B. Diffractive contributions

Here we consider the contributions from purely diffractive fusion processes given by the diagrams of Fig. 2. We have the following fusion processes [see (2.14)]:

$$\mathcal{M}_\mu^{(\mathbb{R}_- -\mathbb{P})} = \mathcal{M}_\mu^{(\mathbb{P}\rho_\mathbb{R})} + \mathcal{M}_\mu^{(\rho_\mathbb{R}\mathbb{P})} + \mathcal{M}_\mu^{(\mathbb{P}\omega_\mathbb{R})} + \mathcal{M}_\mu^{(\omega_\mathbb{R}\mathbb{P})}, \quad (2.18)$$

$$\mathcal{M}_\mu^{(\mathbb{R}_- -\mathbb{R}_+)} = \mathcal{M}_\mu^{(f_{2\mathbb{R}}\rho_\mathbb{R})} + \mathcal{M}_\mu^{(\rho_\mathbb{R} f_{2\mathbb{R}})} + \mathcal{M}_\mu^{(f_{2\mathbb{R}}\omega_\mathbb{R})}$$
$$+ \mathcal{M}_\mu^{(\omega_\mathbb{R} f_{2\mathbb{R}})} + (f_{2\mathbb{R}} \to a_{2\mathbb{R}}), \quad (2.19)$$

$$\mathcal{M}_\mu^{(\mathbb{O}-\mathbb{P})} = \mathcal{M}_\mu^{(\mathbb{P}\mathbb{O})} + \mathcal{M}_\mu^{(\mathbb{O}\mathbb{P})}, \quad (2.20)$$

$$\mathcal{M}_\mu^{(\mathbb{O}-\mathbb{R}_+)} = \mathcal{M}_\mu^{(f_{2\mathbb{R}}\mathbb{O})} + \mathcal{M}_\mu^{(\mathbb{O} f_{2\mathbb{R}})} + (f_{2\mathbb{R}} \to a_{2\mathbb{R}}). \quad (2.21)$$

For these diffractive fusion processes we assume that only the soft Pomeron $\mathbb{P}_1$ contributes. At high c.m. energies $\sqrt{s}$ the $\mathbb{R}_- - \mathbb{R}_+$-fusion processes (2.19) can be safely neglected.

As indicated in Fig. 2 we use here the vector-meson dominance (VMD) approach. We assume that an appropriate vector meson V from the set ρ^0, ω, ϕ is originally formed in the fusion processes with V then converting to the photon. From isospin invariance the following fusion reactions giving such a vector meson V are possible

$$(\mathbb{P}+f_{2\mathbb{R}},\rho_\mathbb{R}) \to \rho^0, \quad (\rho_\mathbb{R},\mathbb{P}+f_{2\mathbb{R}}) \to \rho^0,$$
$$(\mathbb{P}+f_{2\mathbb{R}},\mathbb{O}+\omega_\mathbb{R}) \to \omega,\phi, \quad (\mathbb{O}+\omega_\mathbb{R},\mathbb{P}+f_{2\mathbb{R}}) \to \omega,\phi,$$
$$(a_{2\mathbb{R}},\mathbb{O}+\omega_\mathbb{R}) \to \rho^0, \quad (\mathbb{O}+\omega_\mathbb{R},a_{2\mathbb{R}}) \to \rho^0,$$
$$(a_{2\mathbb{R}},\rho_\mathbb{R}) \to \omega,\phi, \quad (\rho_\mathbb{R},a_{2\mathbb{R}}) \to \omega,\phi. \quad (2.22)$$

Finally the $V \to \gamma$ transition is treated in the standard way; see (3.23)–(3.25) of Ref. [23]. Our *Ansatz* for the $\mathbb{P}\rho_\mathbb{R}\rho$ vertex follows the one for the $\mathbb{P}\rho\rho$ in (3.47) of Ref. [23] with the replacements $a_{\mathbb{P}\rho\rho} \to a_{\mathbb{P}\rho_\mathbb{R}\rho}$, $b_{\mathbb{P}\rho\rho} \to b_{\mathbb{P}\rho_\mathbb{R}\rho}$, and similarly for the $\mathbb{P}\omega_\mathbb{R}\omega$ vertex as well as for $f_{2\mathbb{R}}$ in the place of $\mathbb{P}$. All vertices occurring here were discussed in [23,27,29,34,35] except for $\mathbb{P}\mathbb{O}\omega$, $f_{2\mathbb{R}}\mathbb{O}\omega$, $f_{2\mathbb{R}}\mathbb{O}\phi$, and $a_{2\mathbb{R}}\mathbb{O}\rho^0$. In a first approximation, at the high energies discussed here, we shall set these vertices to zero.
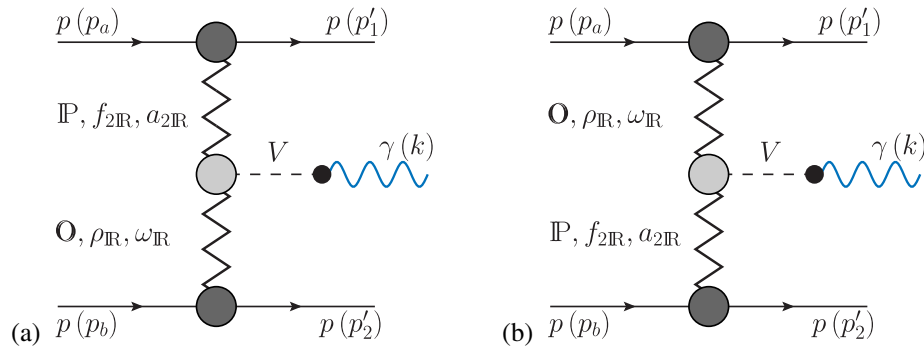

FIG. 2. Diagrams for diffractive production of a photon in high-energy proton-proton collisions via Reggeon, Pomeron, and Odderon exchanges: (a) $(\mathbb{R}_+/\text{Pomeron})$-$(\mathbb{R}_-/\text{Odderon})$ fusion; (b) $(\mathbb{R}_-/\text{Odderon})$-$(\mathbb{R}_+/\text{Pomeron})$ fusion. We use here the vector-meson dominance (VMD) approach and V stands for the appropriate vector meson ρ^0,ω,ϕ which is coupling to the photon according to (2.22).

As an example we discuss one diagram contributing to the $\mathbb{R}_- - \mathbb{P}$ process (2.18). The $\mathbb{P}\rho_{\mathbb{R}}$-exchange amplitude can be written as

$$
\begin{aligned}
\mathcal{M}_\mu^{(\mathbb{P}\rho_{\mathbb{R}})} &= (-i)\bar{u}(p_1', \lambda_1) i\Gamma_{\alpha_1\beta_1}^{(\mathbb{P}pp)}(p_1', p_a) u(p_a, \lambda_a) i\Delta^{(\mathbb{P})\alpha_2\beta_2,\alpha_1\beta_1}(s_1, t_1) i\Gamma_{\sigma_1\kappa_1\alpha_2\beta_2}^{(\mathbb{P}\rho_{\mathbb{R}}\rho)}(k, q_2) \\
&\quad \times i\Delta^{(\rho)\sigma_1\sigma_2}(k) i\Gamma_{\sigma_2\mu}^{(\rho\to\gamma)} i\Delta^{(\rho_{\mathbb{R}})\kappa_1\kappa_2}(s_2, t_2)\bar{u}(p_2', \lambda_2) i\Gamma_{\kappa_2}^{(\rho_{\mathbb{R}}pp)}(p_2', p_b) u(p_b, \lambda_b) \\
&= ie\frac{m_\rho^2}{\gamma_\rho}\Delta_T^{(\rho)}(k^2)\bar{u}(p_1', \lambda_1)\Gamma_{\alpha\beta}^{(\mathbb{P}pp)}(p_1', p_a) u(p_a, \lambda_a)\frac{1}{2s_1}(-is_1\alpha_\mathbb{P}')^{\alpha_\mathbb{P}(t_1)-1} \\
&\quad \times [2a_{\mathbb{P}\rho_{\mathbb{R}}\rho}\Gamma_{\mu\kappa}^{(0)\alpha\beta}(k, -q_2) - b_{\mathbb{P}\rho_{\mathbb{R}}\rho}\Gamma_{\mu\kappa}^{(2)\alpha\beta}(k, -q_2)]F_M(t_1)F_M(t_2)F^{(\rho)}(k^2) \\
&\quad \times \frac{1}{M_-^2}(-is_2\alpha_{\rho_{\mathbb{R}}}')^{\alpha_{\rho_{\mathbb{R}}}(t_2)-1}\bar{u}(p_2', \lambda_2)\Gamma^{(\rho_{\mathbb{R}}pp)\kappa}(p_2', p_b) u(p_b, \lambda_b).
\end{aligned}
\tag{2.23}
$$

For real photons ($k^2 = 0$) we have $\Delta_T^{(\rho)}(k^2) = -1/m_\rho^2$ and $F^{(\rho)}(k^2) = 1$. The $\gamma\rho^0$ coupling γ_ρ is given by (3.23)–(3.25) of Ref. [23]. For the $\mathbb{P}\rho_{\mathbb{R}}\rho$ coupling parameters we assume that $a_{\mathbb{P}\rho_{\mathbb{R}}\rho} = a_{\mathbb{P}\rho\rho}$, $b_{\mathbb{P}\rho_{\mathbb{R}}\rho} = b_{\mathbb{P}\rho\rho}$ and use the values $a_{\mathbb{P}\rho\rho} = 0.45 \text{ GeV}^{-3}$, $b_{\mathbb{P}\rho\rho} = 6.5 \text{ GeV}^{-1}$ from Table 1 of Ref. [27]. We have checked that these parameters give a good description of the HERA data [42,43] for the $\gamma p \to \rho^0 p$ reaction. The $\rho_{\mathbb{R}}\mathbb{P}$-exchange amplitude is obtained from (2.23) with the replacements (2.17).

In a similar way we obtain the $\mathbb{P}\omega_{\mathbb{R}}$- and $\omega_{\mathbb{R}}\mathbb{P}$-exchange amplitudes in (2.18). Here, in the calculations, we include $\phi - \omega$ mixing and we take the coupling parameters found in (B1), (B4), (B10), and (B11) of Ref. [35].

For the amplitude with the Odderon exchange, $\mathcal{M}_\mu^{(\mathbb{O}-\mathbb{P})}$ (2.20), we consider only the two contributions $(\mathbb{O}, \mathbb{P}) \to \phi \to \gamma$ and $(\mathbb{P}, \mathbb{O}) \to \phi \to \gamma$. We use the relations given in Sec. II B of Ref. [35] for the $pp \to pp\phi$ reaction. Thus, the amplitude for the $\mathbb{O}\mathbb{P}$-exchange contribution $\mathcal{M}_\mu^{(\mathbb{O}\mathbb{P})}$ to $pp \to pp\gamma$ is obtained from (2.26) of Ref. [35] by the replacement $i\Gamma_\kappa^{(\phi KK)}(p_3, p_4) \to i\Gamma_\kappa^{(\phi\to\gamma)}$. The same replacement holds for the $\mathbb{P}\mathbb{O}$-exchange amplitude. For the $\mathbb{O} - \mathbb{P}$-fusion processes we shall use the double-Regge-pole *Ansatz* [2] for the Odderon. With this *Ansatz* we were able to describe the ρ parameter, the ratio of the real part to the imaginary part of the forward pp-elastic-scattering amplitude, as measured by the TOTEM [44] and ATLAS [45] Collaborations; see the discussion in Sec. IV A of Ref. [2].

The quantities needed to calculate the fusion amplitudes using the VMD approach were discussed in [23,29,34,35]. In [23] elastic and total $\rho^0 p$ cross sections were discussed. There, the $\mathbb{P}\rho\rho$ and $f_{2\mathbb{R}}\rho\rho$ coupling constants were estimated assuming that at high-energies the total cross section for transversely polarized ρ^0 mesons equals to the average of the $\pi^\pm p$ cross sections. In analogy to the $\rho^0 p$ scattering the elastic and total cross section for ωp and ϕp were treated in [34,35]. From a comparison of our model for the $\gamma p \to V p$ processes to the experimental data, especially those from HERA, the relevant coupling constants and the form-factor parameters for the Pomeron and Reggeon exchanges were found.

We use for the purely diffractive fusion contributions the default values of the Reggeon trajectories from Sec. 3 of Ref. [23], but for the soft Pomeron we take in our calculations $\epsilon_\mathbb{P} = 0.0865$, as determined in [2] by comparison with high-energy pp elastic scattering data, instead of $\epsilon_\mathbb{P} = 0.0808$, the default value from [23]; see the discussion in Appendix A. We also use the exponential Pomeron/Reggeon-proton form factor $F(t) = \exp(-b|t|)$ [instead of $F_1(t)$ given in (3.29) of Ref. [23]] with $b = 2.95 \text{ GeV}^{-2}$ adjusted to the TOTEM data [44,46] on pp elastic scattering for $\sqrt{s} = 13$ TeV (see Fig. 5 of Ref. [2]).

III. RESULTS AND DISCUSSIONS

We start by showing our results for the $pp \to pp\gamma$ reaction from the photon-$\mathbb{P}/\mathbb{R}$-fusion processes. Calculations were done for $\sqrt{s} = 13$ TeV, $0.1 \text{ GeV} < k_\perp < 1$ GeV, and for photon rapidities $|y| < 2.5$. In this kinematic range the soft-Pomeron term ($\mathbb{P}_1$) gives the dominant contribution while the hard-Pomeron term ($\mathbb{P}_0$) and the Reggeon term are negligibly small. There also the FIT 1 (A9) and FIT 2 (A10) parametrizations for the $\mathbb{P}_j\gamma^*\gamma^*$ and $\mathbb{R}_+\gamma^*\gamma^*$ coupling functions hardly differ. In the calculations for the photoproduction contribution we use the FIT 2 parametrization.

In Fig. 3 we show the distributions in y, rapidity of the photon, and in W_1, the subenergy of the γp system. We present the complete result (denoted by "total") and the results corresponding to the diagrams shown in Figs. 1(a) and 1(b) separately. The interference term between the $\gamma\mathbb{P}/\mathbb{R}$ contribution [diagram (a)] and the $\mathbb{P}/\mathbb{R}\gamma$ contribution [diagram (b)] is also shown. This interference effect is destructive.

Figure 4 shows that limiting ourselves to $|y| < 2.5$ and $0.1 \text{ GeV} < k_\perp < 1$ GeV we avoid the low W_1 and low W_2 regions which are a bit less under theoretical control in our model; see the discussion in Sec. II A. The left panel shows the distribution in (W_1, y). The cut at $|y| < 2.5$ eliminates small subenergies W_1 [see (2.2)] and we have $W_1 \geq 10$ GeV. For symmetry reasons the (W_2, y) distribution is obtained by the replacement $(W_1, y) \to (W_2, -y)$. Thus, we also have $W_2 \geq 10$ GeV. In the right panel of Fig. 4 we show the (W_1, W_2) distribution which again
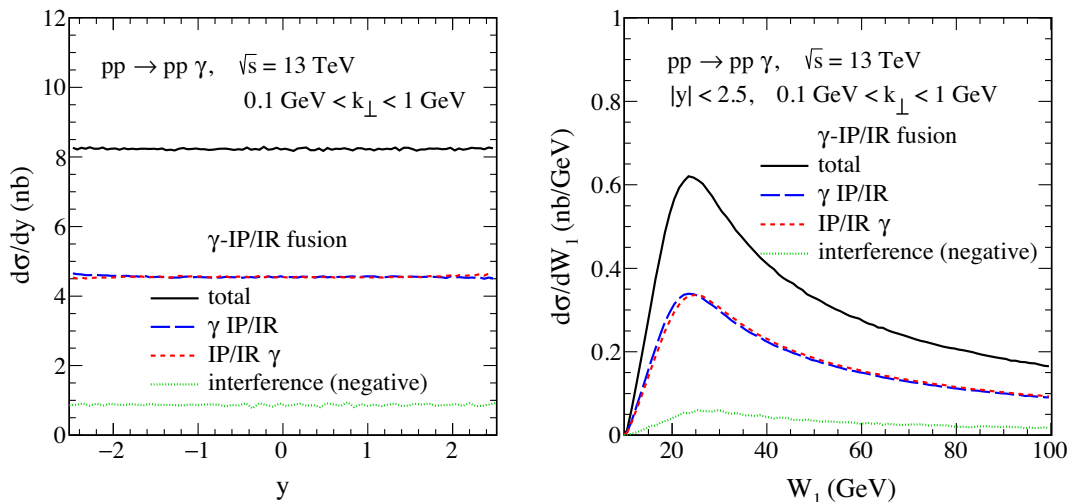
FIG. 3.   The differential distributions in the rapidity of the photon and in the subenergy W_1 of the γp system for the $pp \to pp\gamma$ reaction via the $\gamma - \mathbb{P}/\mathbb{R}$-fusion processes. The calculations were done for $\sqrt{s} = 13$ TeV and with cuts on $|y| < 2.5$ and 0.1 GeV $< k_\perp < 1$ GeV. The solid line corresponds to the complete result (total), the blue long-dashed and red dashed lines correspond to the $\gamma\mathbb{P}/\mathbb{R}$ contribution [see Fig. 1(a)] and the $\mathbb{P}/\mathbb{R}\gamma$ contribution [see Fig. 1(b)], respectively. The destructive interference term is shown separately by the green dotted line.
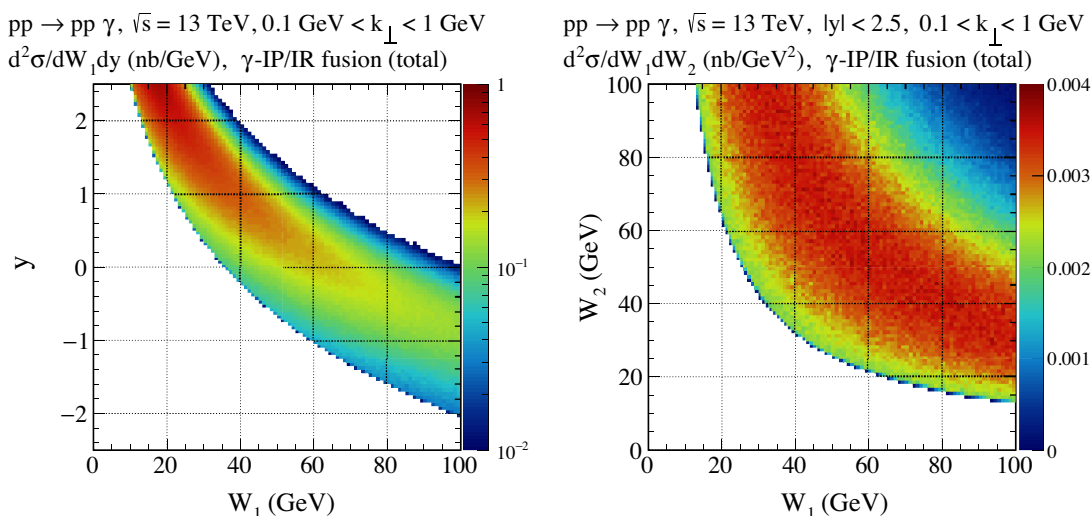

FIG. 4.   The two-dimensional distributions in (W_1, y) and (W_1, W_2) for the $pp \to pp\gamma$ reaction via the $\gamma - \mathbb{P}/\mathbb{R}$-fusion processes. The calculations were done for $\sqrt{s} = 13$ TeV and with cuts on $|y| < 2.5$ and 0.1 GeV $< k_\perp < 1$ GeV.

shows very clearly that with our cuts we avoid the regions of small W_1 and/or W_2.

We also find small enhancements at photon rapidities $|y| \simeq 2.5$, which correspond to low-$W_{1,2}$ regions (see Fig. 4). This effect is due to the Reggeon component and its constructive interference with the soft-Pomeron[2];

---

[2]Note that another constructive interference effect, namely that between the soft- and hard-Pomeron components, plays an important role in the description of HERA DVCS data in the process $\gamma^*(Q^2)p \to \gamma p$, especially for large photon virtualities Q^2; see e.g. Fig. 4 of Ref. [40]. The Reggeon contribution is negligibly small there.

see the left panel of Fig. 3. This effect is more visible in Fig. 9 below for photoproduction at $|y| \simeq 4$.

In Fig. 5 we present the distributions in $k_\perp$ and ω. Again we show the complete result (total), the $\gamma\mathbb{P}/\mathbb{R}$ and $\mathbb{P}/\mathbb{R}\gamma$ terms, and the interference term between them. The cross sections $d\sigma/dk_\perp$ and $d\sigma/d\omega$ gradually increase and reach maxima at $k_\perp \simeq 0.25$ GeV and at $\omega \simeq 0.4$ GeV, respectively. After that both distributions decrease quickly with increasing $k_\perp$ and ω.

In Fig. 6 we show the two-dimensional differential cross sections in the $W_{1,2}$-$k_\perp$ plane (the left panel) and in the ω-$k_\perp$ plane (the right panel) calculated for $|y| < 2.5$. In the right panel, large $|y|$ is near the ω axis, and $y = 0$
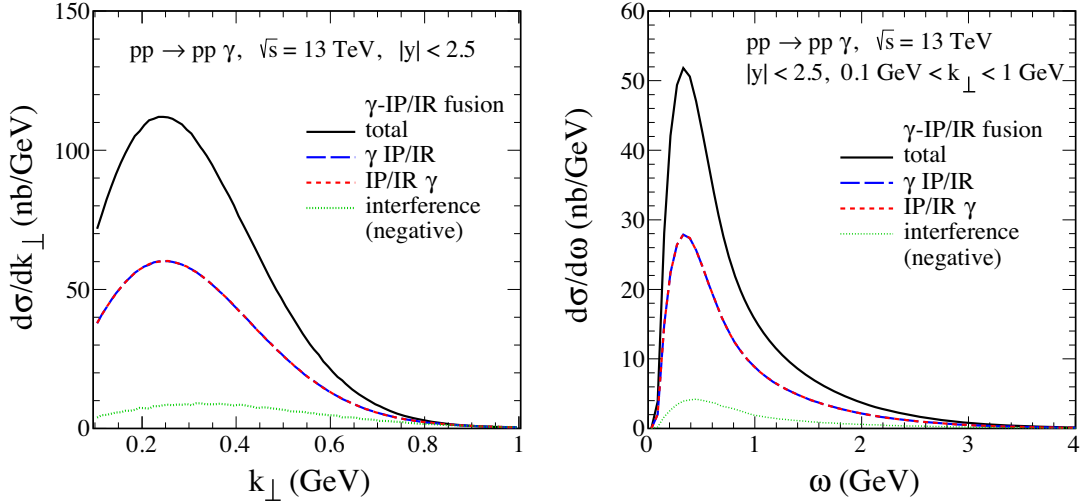
FIG. 5.   The differential distributions in transverse momentum of the photon and in the energy of the photon for the $pp \to pp\gamma$ reaction via the $\gamma - \mathbb{P}/\mathbb{R}$-fusion processes. The calculations were done for $\sqrt{s} = 13$ TeV and with cuts on $|y| < 2.5$ and 0.1 GeV $< k_\perp < 1$ GeV. The meaning of the lines is the same as in Fig. 3.
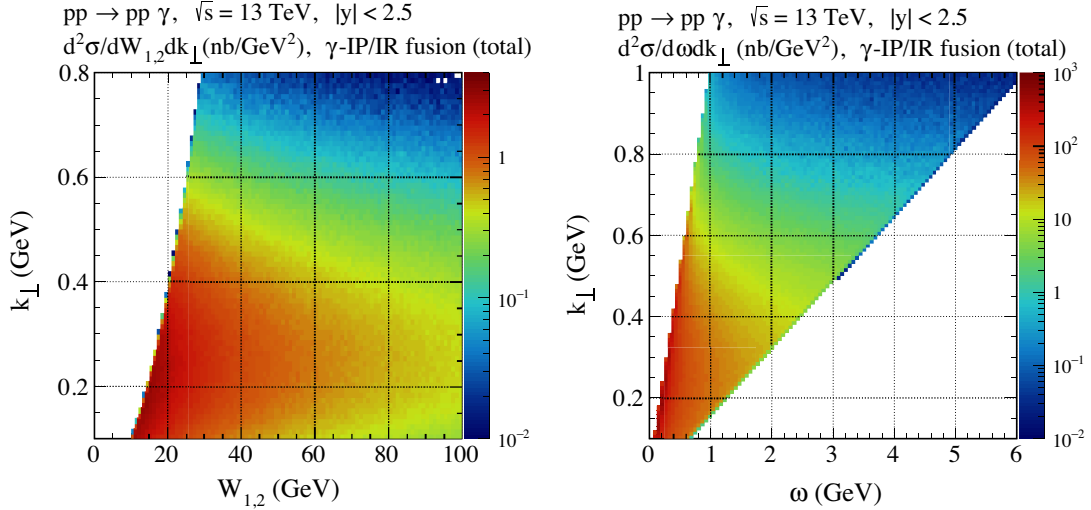

FIG. 6.   The two-dimensional distributions in $(W_{1,2}, k_\perp)$ and $(\omega, k_\perp)$ for the $pp \to pp\gamma$ reaction via the $\gamma - \mathbb{P}/\mathbb{R}$-fusion processes. The calculations were done for $\sqrt{s} = 13$ TeV and $|y| < 2.5$.

corresponds to $\omega = k_\perp$. The phase-space region $\omega < k_\perp$ is forbidden.

In Fig. 7 we show the distributions in transverse momentum of the proton $p(p'_1)$ (here $p_{t,1} = |\mathbf{p}'_{t,1}|$), in four-momentum transfer squared (t_1), and in $\Delta p_{t,p}$ defined as

$$\Delta p_{t,p} = |\mathbf{p}'_{t,1}| - |\mathbf{p}'_{t,2}|. \tag{3.1}$$

Figures 7(a) and 7(b) show that the low-$p_{t,1}$ region is dominated by the photon exchange in the $\gamma\mathbb{P}/\mathbb{R}$ term. This is caused by the factor $1/t_1$ for $\gamma\mathbb{P}/\mathbb{R}$ from the photon propagator. In Fig. 7(c), the region of intermediate $|t_1|$, 0.01 GeV$^2 < |t_1| < 1$ GeV^2, is governed by the Pomeron

exchange in the $\mathbb{P}/\mathbb{R}\gamma$ term. Not shown is the large-$|t_1|$ region, $|t_1| > 1$ GeV^2. We find that there again the $\gamma\mathbb{P}/\mathbb{R}$ term dominates. This is due to the $1/|t_1|$ fall-off of the photon propagator in the $\gamma\mathbb{P}/\mathbb{R}$ term winning over the exponential fall-off in $|t_1|$ of the Pomeron part in the $\mathbb{P}/\mathbb{R}\gamma$ term. Note that for the CEP of a photon we find $|t_1|$ and $p_{t,1}$ distributions which are strongly peaked at very small $|t_1|$ and $p_{t,1}$, respectively. In contrast, for the diffractive bremsstrahlung mechanism photons hardly contribute to very small values of $p_{t,p}$ and $d\sigma/dp_{t,p}$ reaches a maximum at $p_{t,p} \sim \sqrt{|t_{1,2}|} \sim 0.3$ GeV; see Fig. 7 of Ref. [2]. The $\Delta p_{t,p}$ distribution shown in Fig. 7(d) is interesting as there the destructive interference between the two terms $\gamma\mathbb{P}/\mathbb{R}$ and $\mathbb{P}/\mathbb{R}\gamma$ is sizeable around $\Delta p_{t,p} = 0$.
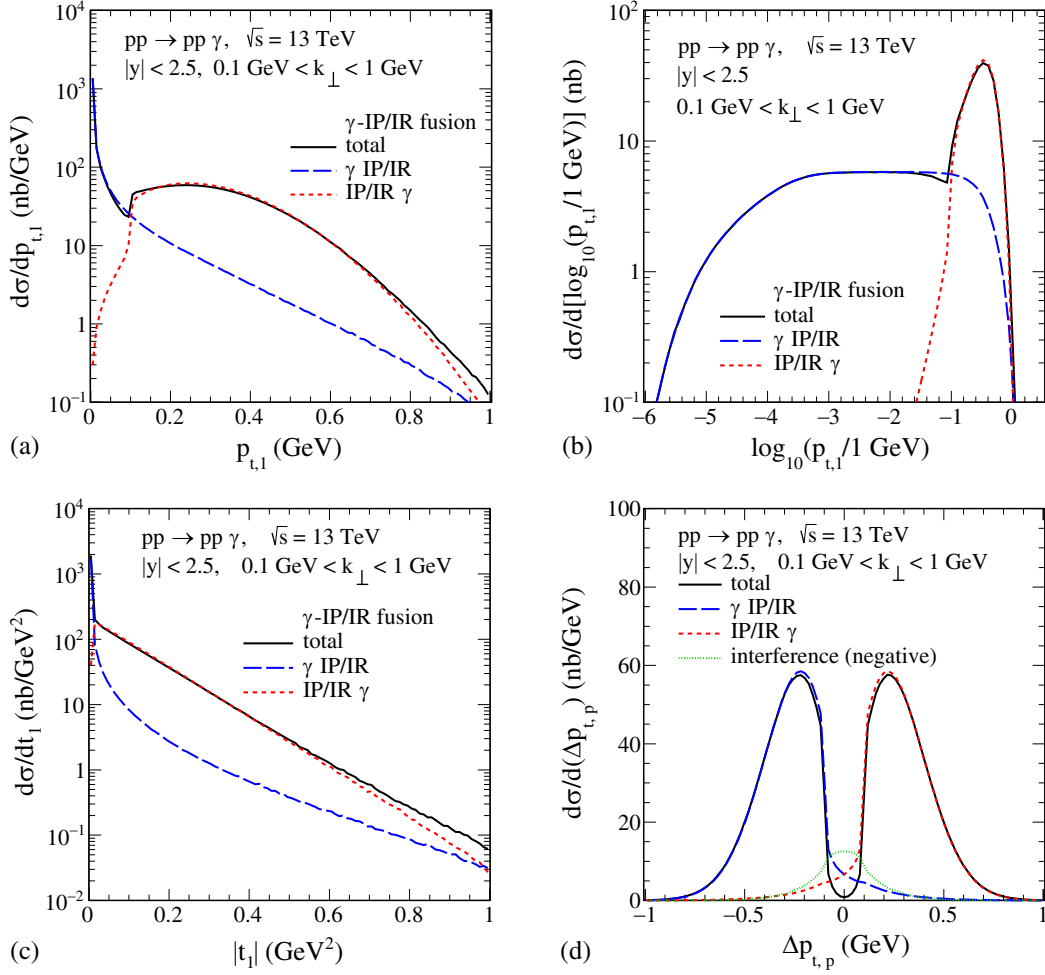
FIG. 7.   The differential distributions in transverse momentum of the proton $p(p'_1)$, in four-momentum transfer squared $|t_1|$, and in $\Delta p_{t,p} = |\boldsymbol{p}'_{t,1}| - |\boldsymbol{p}'_{t,2}|$ for the $pp \to pp\gamma$ reaction via the $\gamma - \mathbb{P}/\mathbb{R}$-fusion processes. The calculations were done for $\sqrt{s} = 13$ TeV and with cuts on $|y| < 2.5$ and 0.1 GeV $< k_\perp < 1$ GeV. The meaning of the lines is the same as in Fig. 3.

In Fig. 8 we show the two-dimensional distributions in $(t_1, k_\perp^2)$. The results for the two diagrams shown in Fig. 1 and for their coherent sum (total) are presented. From transverse momentum conservation the transverse momentum of the final state photon is the vector sum of the transverse momenta of virtual photon and Pomeron/Reggeon. The plots of Fig. 8 are easily understood. For the $\gamma\mathbb{P}/\mathbb{R}$ term the photon propagator in Fig. 1(a) forces the proton $p(p'_1)$ to go out with very small transverse momentum, $|\boldsymbol{p}'_{t,1}|^2 \approx -t_1 \approx 0$. Then the proton $p(p'_2)$ will have $|\boldsymbol{p}'_{t,2}|^2 \approx |\boldsymbol{k}_\perp|^2$ and this ranges up to $|\boldsymbol{k}_\perp|^2 \approx 1$ GeV^2; see Fig. 8(a). For the $\mathbb{P}/\mathbb{R}\gamma$ term we will correspondingly have $|\boldsymbol{p}'_{t,2}|^2 \approx 0$ and $|\boldsymbol{p}'_{t,1}|^2 \approx -t_1 \approx |\boldsymbol{k}_\perp|^2$. This is indeed what is seen in Fig. 8(b). In Fig. 8(c) we see the combination of these two effects.

Finally, we compare the results for the $pp \to pp\gamma$ reaction from the fusion processes (CEP) discussed in this article with the results corresponding to the diffractive bremsstrahlung discussed in [2]. We consider separately the bremsstrahlung, the photoproduction $\gamma - \mathbb{P}/\mathbb{R}$, and the two diffractive contributions $\mathbb{R}_- - \mathbb{P}$ and $\mathbb{O} - \mathbb{P}$. We denote, for brevity, the coherent sum of the contributions $\gamma\mathbb{P}$ and $\mathbb{P}\gamma$ by $\gamma - \mathbb{P}$, the coherent sum of $\gamma\mathbb{R}_+$ and $\mathbb{R}_+\gamma$ by $\gamma - \mathbb{R}_+$, and the complete photoproduction contribution by $\gamma - \mathbb{P}/\mathbb{R}$. The analogous shorthand notation is used also for other contributions, $\mathbb{R}_- - \mathbb{P}$ and $\mathbb{O} - \mathbb{P}$.

In Fig. 9 we compare different processes for the $pp \to pp\gamma$ reaction calculated for $\sqrt{s} = 13$ TeV, and a somewhat larger range of photon rapidities $|y| < 4$, and for two $k_\perp$ intervals as specified in the figure legends. We see that the photoproduction is the dominant process for $k_\perp > 10$ MeV, its cross section $d\sigma/dk_\perp$ gradually increases and reaches a maximum at $k_\perp \simeq 0.25$ GeV. The diffractive bremsstrahlung contribution is most important in the area of small $k_\perp$ but its cross section decreases with increasing $k_\perp$. The other purely diffractive contributions, $\mathbb{R}_- - \mathbb{P}$ and $\mathbb{O} - \mathbb{P}$, give much smaller cross sections.

As was mentioned in [2] the intermediate protons in the bremsstrahlung-type diagrams are off shell when the final
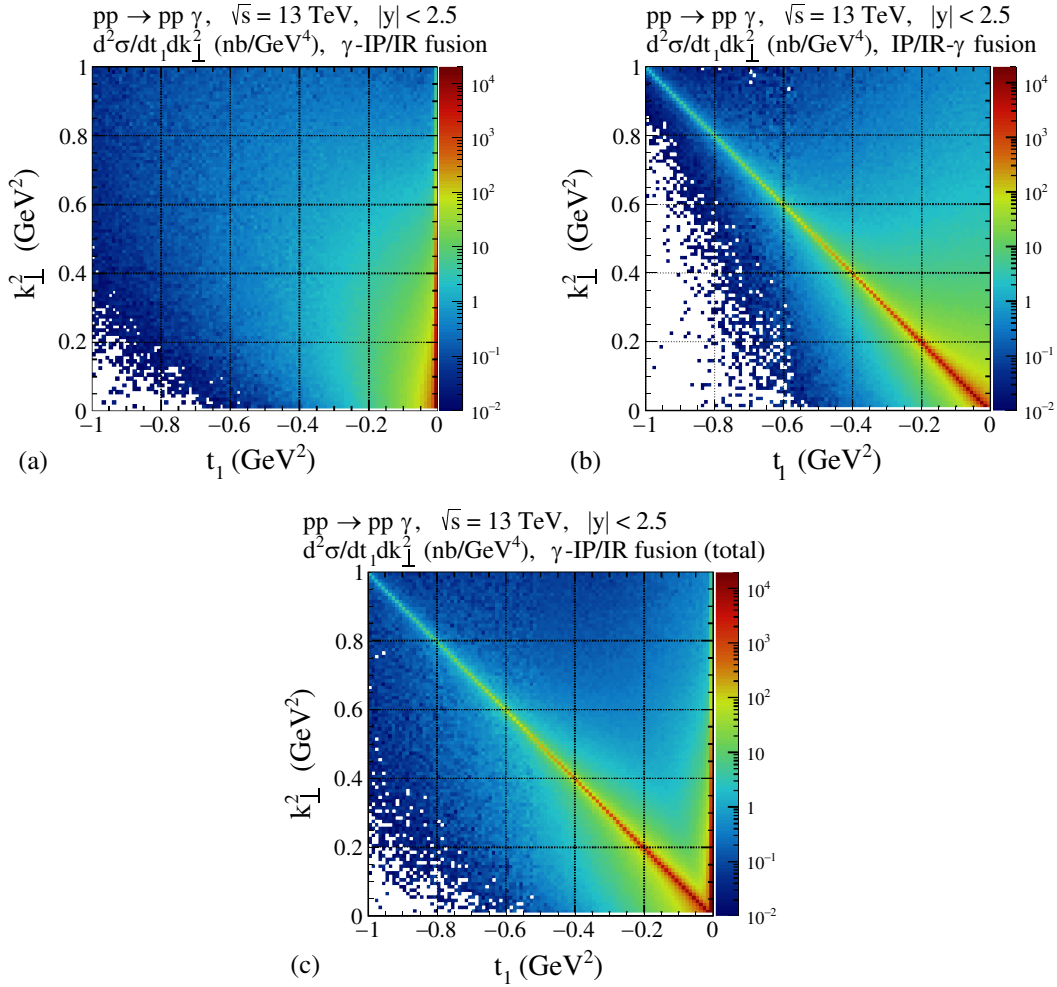
FIG. 8. The two-dimensional distributions in $(t_1, k_\perp^2)$ for the $pp \to pp\gamma$ reaction. The calculations were done for $\sqrt{s} = 13$ TeV and with cuts on $|y| < 2.5$ and 0.1 GeV $< k_\perp < 1$ GeV. The top left panel shows the result for only the diagram (a) of Fig. 1 and the top right panel for the diagram (b) of Fig. 1. The bottom panel shows the complete result for the $\gamma - \mathbb{P}/\mathbb{R}$-fusion processes.

state photon is emitted from an external proton line. But in our model of the bremsstrahlung contributions we set possible form factors for off-shell protons in the vertices and in the proton propagator to 1. We expect that up to $k_\perp \simeq 0.1$ GeV and small ω the off-shell effects should be small.[3] Taking this into account, we do not show here results for the bremsstrahlung mechanism for a larger $k_\perp$ range where our estimates are uncertain.

It is a known fact that absorption effects due to strong proton-proton interactions have much more influence on the purely diffractive processes than on the photoproduction processes; see e.g. Table II of Ref. [35] where the ratios of full and Born cross sections for the $pp \to pp\phi$ reaction for the $\gamma - \mathbb{P}$- and $\mathbb{O} - \mathbb{P}$-fusion processes are shown. Thus, it can be expected that for the $pp \to pp\gamma$ reaction at not too large $k_\perp$ the absorption is small for the $\gamma - \mathbb{P}/\mathbb{R}$-fusion processes.

It is interesting to note that the $\gamma - \mathbb{P}/\mathbb{R}$-fusion processes are of the same order in $\alpha_{\rm em}$ as the bremsstrahlung-type processes via the photon exchange, which we call the QED bremsstrahlung; see Table I. In the case of the photon production via QED bremsstrahlung $d\sigma/dt_{1,2}$ increases for $t_{1,2} \to 0$ due to the photon propagator which is proportional to $1/t$. We have checked that for the kinematics considered in our paper the QED-bremsstrahlung cross section is about a factor of 200 smaller than the diffractive bremsstrahlung cross section via the Pomeron exchange. For these two bremsstrahlung mechanisms, the shapes of the distributions in y, $k_\perp$, and ω are similar.

In Fig. 10 we present the distributions in $\Delta p_{t,p} = |\boldsymbol{p}'_{t,1}| - |\boldsymbol{p}'_{t,2}|$ for the low-$k_\perp$ region and for two $|y|$ intervals for the $pp \to pp\gamma$ reaction. We compare the $\gamma - \mathbb{P}/\mathbb{R}$-fusion processes to diffractive bremsstrahlung-type emission of photons discussed in [2]. We see from Figs. 9 and 10 that these contributions have different characteristics in $k_\perp$ and $\Delta p_{t,p}$ and that the relative size of the cross sections depends on the photon-rapidity range. The physics behind
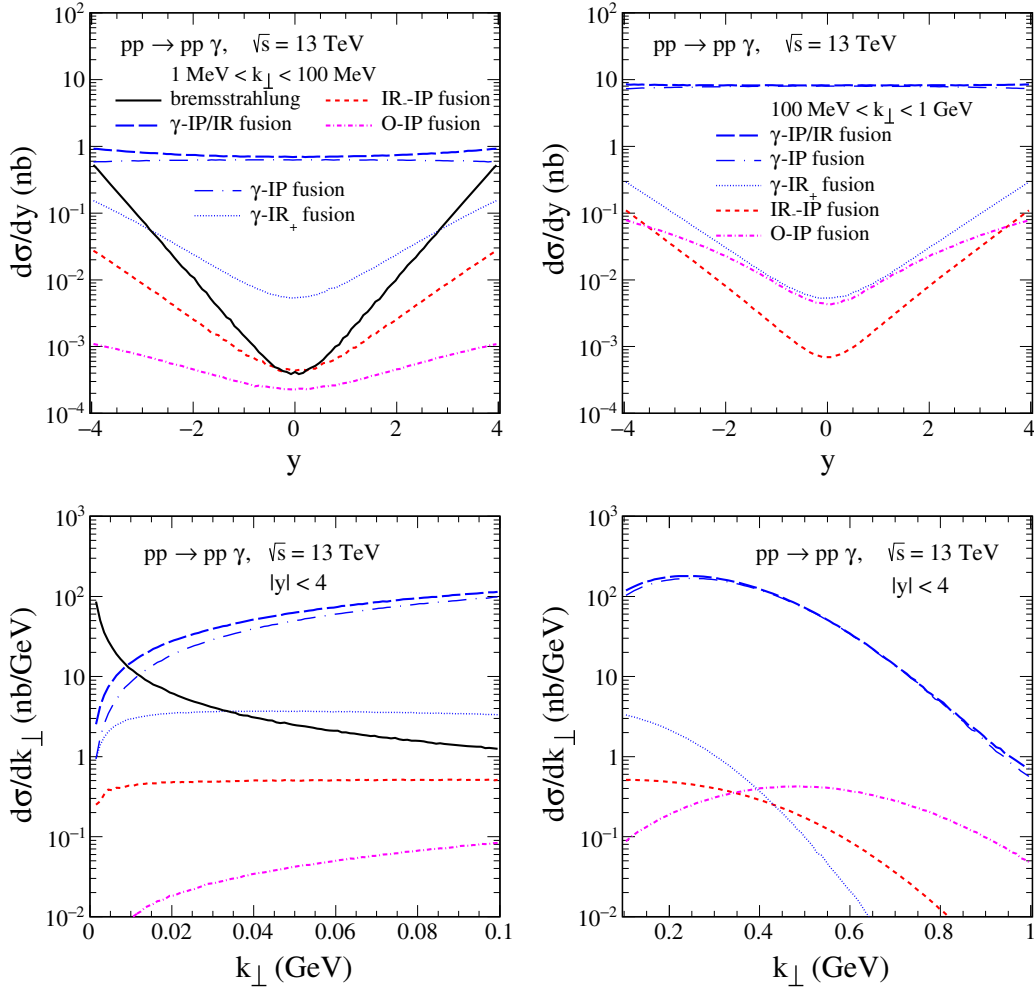
---

[3]We refer the reader to Figs. 8 and 17 of Ref. [2] where the results for $k_\perp$ up to 0.4 GeV are shown.

FIG. 9.   The differential distributions for the $pp \rightarrow pp\gamma$ reaction calculated for $\sqrt{s} = 13$ TeV, $|y| < 4$, 1 MeV $< k_\perp <$ 100 MeV (left panels) and 100 MeV $< k_\perp <$ 1 GeV (right panels). The black solid line corresponds to the diffractive bremsstrahlung, the blue long-dash-dotted line to the $\gamma - \mathbb{P}$-fusion processes ($\gamma\mathbb{P} + \mathbb{P}\gamma$), the blue dotted line to the $\gamma - \mathbb{R}_+$-fusion processes ($\gamma\mathbb{R}_+ + \mathbb{R}_+\gamma$), and the blue long-dashed line to the coherent sum of all photoproduction contributions. The red dashed line corresponds to the $\mathbb{R}_- - \mathbb{P}$-fusion processes while the magenta dash-dotted line to the $\mathbb{O} - \mathbb{P}$ contribution.
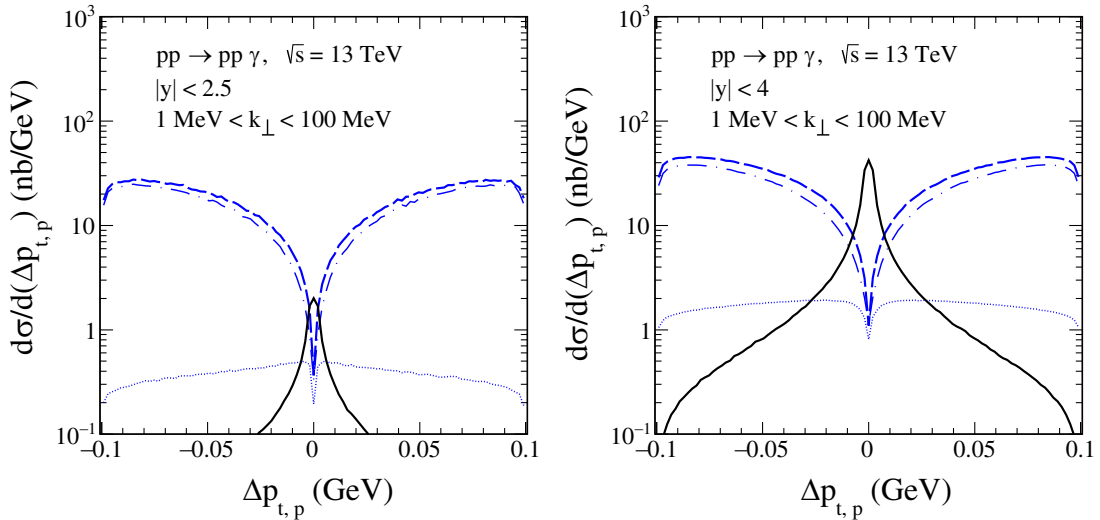

FIG. 10.   The distributions in $\Delta p_{t,p}$ for the $\gamma - \mathbb{P}/\mathbb{R}$-fusion processes (blue lines) and diffractive bremsstrahlung (black lines). The meaning of the lines is the same as in Fig. 9. The calculations were done for $\sqrt{s} = 13$ TeV, 1 MeV $< k_\perp <$ 100 MeV, and for two $|y|$ intervals as specified in the figure legends.

the results shown in Fig. 10 is as follows. In the discussion of the results of Fig. 8 we saw that in the CEP process we have either $|\boldsymbol{p}'_{t,1}| \approx 0$, $|\boldsymbol{p}'_{t,2}|$ sizeable, or $|\boldsymbol{p}'_{t,2}| \approx 0$, $|\boldsymbol{p}'_{t,1}|$ sizeable. This explains the double-hump structure of the CEP curves in Fig. 10. For bremsstrahlung, on the other hand, the kinematics of the $pp \to pp\gamma$ reaction is close to that for elastic scattering, $pp \to pp$, where $|\boldsymbol{p}'_{t,1}| = |\boldsymbol{p}'_{t,2}|$. We expect, therefore, also for bremsstrahlung $|\boldsymbol{p}'_{t,1}| \approx |\boldsymbol{p}'_{t,2}|$ and, thus, $\Delta p_{t,p} \approx 0$. And this is indeed what we see from Fig. 10. Furthermore, we see from Fig. 9, upper left panel, that bremsstrahlung increases relative to CEP for larger $|y|$. And this can also be seen by comparing the left and right panels of Fig. 10. We conclude by emphasizing that the measurement of outgoing protons, necessary to obtain distributions as shown in Fig. 10, would allow us to better understand the role of CEP versus bremsstrahlung processes. Hopefully, the ATLAS and CMS Collaborations will be able to measure photons in coincidence with protons in the forward detectors.

IV. CONCLUSIONS

In this paper we have studied diffractive production of photons via different fusion processes within the tensor-Pomeron approach in the reaction $pp \to pp\gamma$ (2.1) at the c.m. energy $\sqrt{s} = 13$ TeV. We have discussed central-exclusive production (CEP) of photons from the photo-production processes given by the diagrams of Fig. 1 and the purely diffractive fusion processes given by the diagrams of Fig. 2. We can only speak of this CEP mechanism if the γp subenergies W_1 and W_2 [see (2.2)] are large enough. We assured this by a cut in the photon rapidity, $|y| < 2.5$, and transverse momentum, 0.1 GeV $< k_\perp < 1$ GeV.

The photoproduction is the dominant CEP mechanism without considering kinematic cuts on the leading protons. Due to the virtual photon exchange one of the protons is scattered at very small angles (very forward/backward proton rapidities). The $\gamma - \mathbb{P}$ exchanges (2.15) populate preferentially the midrapidity region. The subleading $\gamma - \mathbb{R}_+$ exchanges play a role at more forward/backward photon rapidities, when the energies of the subprocesses $\gamma^* p \to \gamma p$ are smaller than for $y \approx 0$; see Fig. 4. Both, $\mathbb{P}$ and $\mathbb{R}_+ = f_{2\mathbb{R}}, a_{2\mathbb{R}}$ exchange are treated as effective tensor exchanges in our model. The complete photoproduction result indicates a constructive interference effect of $\gamma - \mathbb{P}$- and $\gamma - \mathbb{R}_+$-fusion processes. There is, on the other hand, sizeable destructive interference between the two terms $\gamma\mathbb{P}/\mathbb{R}$ and $\mathbb{P}/\mathbb{R}\gamma$ corresponding to the diagrams shown in Figs. 1(a) and 1(b), respectively; see Fig. 5.

We have compared the CEP processes to standard results for bremsstrahlung-type emission of soft photons discussed previously in [2]. We have shown that the photoproduction contribution wins over the bremsstrahlung one for $|y| < 4$ and $k_\perp \gtrsim 10$ MeV (see Fig. 9). The cross section $d\sigma/dk_\perp$ for the $\gamma - \mathbb{P}/\mathbb{R}$-fusion processes gradually increases and

reaches a maximum at $k_\perp \simeq 0.25$ GeV. The purely diffractive CEP fusion processes, $\mathbb{R}_- - \mathbb{P}$ and $\mathbb{O} - \mathbb{P}$, give much smaller cross sections there. For the photon brems-strahlung, discussed in [2], the cross section for $k_\perp \to 0$ diverges as $1/k_\perp$.

To summarize: in this article we have studied central-exclusive production of single photons in proton-proton collisions at LHC energies, $\sqrt{s} = 13$ TeV. The CEP process with $\gamma - \mathbb{P}$ fusion is the most important one and preferentially produces photons at midrapidity. In this kinematic region CEP dominates over photons produced by diffractive bremsstrahlung. And this is true despite the fact that CEP with $\gamma - \mathbb{P}$ fusion is of higher order in $\alpha_{\rm em}$ compared to diffractive bremsstrahlung. It is clear that our studies can easily be adapted to pp collisions at RHIC energies, $\sqrt{s} = 200$–510 GeV.

We hope that our theoretical studies of the $pp \to pp\gamma$ reaction will find experimental counterparts by measurements of soft photons at RHIC and at the LHC. We emphasize that for detailed comparisons of our predictions with experiment measurement of the outgoing protons would be most welcome.

APPENDIX A: EFFECTIVE PROPAGATOR AND VERTEX FUNCTIONS

We give here a list of all effective propagator and vertex functions used in the calculation of the $\gamma - \mathbb{P}/\mathbb{R}$-fusion processes discussed in Sec. II A.

For the two tensor Pomerons, soft $(j = 1)$ and hard $(j = 0)$, we use the effective propagators and the $\mathbb{P}_j pp$ vertices as given in Appendix A of Ref. [26],

$$
i\Delta^{(\mathbb{P}_j)}_{\mu\nu,\kappa\lambda}(s,t)
$$
$$
= \frac{1}{4s}\left(g_{\mu\kappa}g_{\nu\lambda} + g_{\mu\lambda}g_{\nu\kappa} - \frac{1}{2}g_{\mu\nu}g_{\kappa\lambda}\right)(-is\tilde{\alpha}'_j)^{\alpha_j(t)-1}, \quad (A1)
$$

$$
i\Gamma^{(\mathbb{P}_j pp)}_{\mu\nu}(p', p)
$$
$$
= -i3\beta_{jpp}F_1^{(j)}(t)\left\{\frac{1}{2}[\gamma_\mu(p' + p)_\nu + \gamma_\nu(p' + p)_\mu]\right.
$$
$$
\left. - \frac{1}{4}g_{\mu\nu}(\not{p}' + \not{p})\right\}. \quad (A2)
$$

Here $\beta_{1pp} = \beta_{0pp} = 1.87$ GeV^{-1} are coupling constants and $F_1^{(j)}(t)$ are form factors [see Eq. (A11) below]. The *Ansätze* for effective propagators and vertices for the tensor

Reggeons $f_{2\mathbb{R}}$ and $a_{2\mathbb{R}}$ have the same structure as (A1) and (A2), respectively. The contributions of these Reggeons are combined into one term $\mathbb{R}_+$, labeled $j = 2$, and the coupling constant for $\mathbb{R}_+ pp$ is given as $\beta_{2pp} = 3.68$ GeV^{-1}; see (A29) of Ref. [26]. The Pomeron and Reggeon trajectory functions are assumed to be of linear form

$$\alpha_j(t) = \alpha_j(0) + \alpha'_j t, \quad \alpha_j(0) = 1 + \epsilon_j, \quad j = 0, 1, 2. \quad (A3)$$

The values of the intercept parameters of the Regge trajectories obtained in [26] from a comparison to HERA DIS data are

$$\epsilon_1 = 0.0935\left(^{+76}_{-64}\right), \quad \epsilon_0 = 0.3008\left(^{+73}_{-84}\right), \quad \alpha_2(0) = 0.485\left(^{+88}_{-90}\right). \quad (A4)$$

For the slope parameters default values were used in [26] $\alpha'_1 = \alpha'_0 = 0.25$ GeV^{-2}, and $\alpha'_2 = 0.9$ GeV^{-2}, and the scale parameters $\tilde{\alpha}'_j$ were chosen equal to the slope parameters α'_j. In our present work, in the calculation of the $\gamma - \mathbb{P}/\mathbb{R}$ CEP process, we use the above central values for ϵ_1, ϵ_0, and $\alpha_2(0)$ and the default values for α'_j ($j = 0, 1, 2$). In the calculation of the purely diffractive contributions, discussed in Sec. II B, for ϵ_1 we use the value $\epsilon_1 = 0.0865$ as determined by us in [2]. This latter value is about 1 s.d. lower than the value from (A4). The default value from [23,47] is $\epsilon_1 = 0.0808$ which is 2 s.d. lower than the one from (A4). We can motivate our use of different values of ϵ_1 for the different processes shown in Figs. 1 and 2 as follows. In the diagrams of Fig. 1 the Pomeron exchange is in the subreaction $\gamma^* p \to \gamma p$ and we think that it is appropriate to use there the value of ϵ_1 from (A4) as determined from the closely related process $\gamma^* p \to \gamma^* p$; see Ref. [26]. In Fig 2, on the other hand, we have a diffractive collision being close to pp elastic scattering where we determined a slightly lower value of ϵ_1 in [2]. We could, for instance, consider this slightly lower value of ϵ_1 in the hadronic diffraction case as being due to stronger absorption effects there compared to the $\gamma^* p \to \gamma^* p$ reaction.

In any case, in the kinematical range considered by us here the diffractive contribution to the CEP of a single photon is small; see Fig. 9.

The *Ansätze* for the $\mathbb{P}_j \gamma^* \gamma^*$ and $\mathbb{R}_+ \gamma^* \gamma^*$ coupling functions for both real and virtual photons are given in [26]. The $\mathbb{P}_j \gamma^* \gamma^*$ ($j = 0, 1$) vertex reads

$$i\Gamma^{(\mathbb{P}_j \gamma^* \gamma^*)}_{\mu\nu\kappa\rho}(q', q) = i[2a_{j\gamma^*\gamma^*}(q^2, q'^2, t)\Gamma^{(0)}_{\mu\nu\kappa\rho}(q', -q) \\ - b_{j\gamma^*\gamma^*}(q^2, q'^2, t)\Gamma^{(2)}_{\mu\nu\kappa\rho}(q', -q)], \quad (A5)$$

where $t = (q - q')^2$. The rank-4 tensor functions are defined in (A13) and (A14) of Ref. [26],

$$\Gamma^{(0)}_{\mu\nu\kappa\lambda}(k_1, k_2) = [(k_1 \cdot k_2)g_{\mu\nu} - k_{2\mu}k_{1\nu}] \\ \times \left[k_{1\kappa}k_{2\lambda} + k_{2\kappa}k_{1\lambda} - \frac{1}{2}(k_1 \cdot k_2)g_{\kappa\lambda}\right], \quad (A6)$$

$$\Gamma^{(2)}_{\mu\nu\kappa\lambda}(k_1, k_2) = (k_1 \cdot k_2)(g_{\mu\kappa}g_{\nu\lambda} + g_{\mu\lambda}g_{\nu\kappa}) \\ + g_{\mu\nu}(k_{1\kappa}k_{2\lambda} + k_{2\kappa}k_{1\lambda}) \\ - k_{1\nu}k_{2\lambda}g_{\mu\kappa} - k_{1\nu}k_{2\kappa}g_{\mu\lambda} \\ - k_{2\mu}k_{1\lambda}g_{\nu\kappa} - k_{2\mu}k_{1\kappa}g_{\nu\lambda} \\ - [(k_1 \cdot k_2)g_{\mu\nu} - k_{2\mu}k_{1\nu}]g_{\kappa\lambda}. \quad (A7)$$

The $\mathbb{R}_+ \gamma^* \gamma^*$ vertex for real and virtual photons has the same structure as shown in (A5) with $j = 2$; see (A27)–(A31) of Ref. [26]. The coupling functions $a_{j\gamma^*\gamma^*}(q^2, q'^2, t)$ and $b_{j\gamma^*\gamma^*}(q^2, q'^2, t)$, for the case $q^2 = -Q^2$, $q'^2 = 0$, are taken as in (2.21)–(2.23) of Ref. [40],

$$a_{j\gamma^*\gamma^*}(q^2, 0, t) = e^2 \hat{a}_j(Q^2) F^{(j)}(t), \quad j = 0, 1, 2, \\ b_{2\gamma^*\gamma^*}(q^2, 0, t) = e^2 \hat{b}_2(Q^2) F^{(2)}(t). \quad (A8)$$

For two alternative fits for $b_{1\gamma^*\gamma^*}$ and $b_{0\gamma^*\gamma^*}$ we obtained from a comparison to HERA DVCS data

$$\text{FIT 1}: b_{1\gamma^*\gamma^*}(q^2, 0, t) = e^2 \hat{b}_1(0)(1 + Q^2/\Lambda_1^2)^{-1.2} F^{(1)}(t), \quad \Lambda_1 = 1.4 \text{ GeV},$$
$$b_{0\gamma^*\gamma^*}(q^2, 0, t) = e^2 \hat{b}_0(Q^2) F^{(0)}(t), \quad (A9)$$

$$\text{FIT 2}: b_{1\gamma^*\gamma^*}(q^2, 0, t) = e^2 \hat{b}_1(0)(1 + Q^2/\Lambda_2^2)^{-2.0} F^{(1)}(t), \quad \Lambda_2 = 2.0 \text{ GeV},$$
$$b_{0\gamma^*\gamma^*}(q^2, 0, t) = \begin{cases} e^2 \hat{b}_0(Q^2) F^{(0)}(t) & \text{for } Q^2 < 1.5 \text{ GeV}^2 \\ e^2 \Lambda_0 (1 + Q^2/\Lambda_3^2)^{-0.6} F^{(0)}(t) & \text{for } Q^2 \geq 1.5 \text{ GeV}^2 \end{cases},$$
$$\Lambda_0 = 9.46 \times 10^{-3} \text{ GeV}^{-1}, \quad \Lambda_3 = 2.3 \text{ GeV}. \quad (A10)$$

See (2.21)–(2.23) of Ref. [40]. The coupling functions $\hat{a}_j(Q^2)$ and $\hat{b}_j(Q^2)$ were determined in [26] from the global fit to HERA inclusive DIS data for $Q^2 < 50$ GeV^2 and $x < 0.01$ and the ($Q^2 = 0$) photoproduction data. According to [26], for the R_+-Reggeon term, $\hat{a}_2(Q^2) = 0$ while the function $\hat{b}_2(Q^2)$ vanishes rapidly with increasing Q^2. All coupling functions $\hat{a}_j$ and $\hat{b}_j$ are plotted in Fig. 2 of Ref. [40]. For small Q^2, the soft Pomeron function $b_{1\gamma^*\gamma^*}$ gives a larger contribution to the cross section than the corresponding hard one $b_{0\gamma^*\gamma^*}$. In the large Q^2 region the reverse is found.

We use the combined form-factor functions for a given j ($j = 0, 1, 2$)

$$F_{\text{eff}}^{(j)}(t) = F^{(j)}(t) \times F_1^{(j)}(t) = \exp(-b_j|t|/2), \quad \text{(A11)}$$

assuming the same t dependence for both a and b coupling functions. We take $b_1 = b_2 = 5.0$ GeV^{-2} and $b_0 = 1.0$ GeV^{-2} from [40].

APPENDIX B: ESTIMATE OF THE CROSS SECTION FOR $pp \to pp\gamma$ USING THE METHOD OF THE EQUIVALENT PHOTON FLUX

In this appendix we estimate the cross section for the $\gamma\mathbb{P}$ fusion contribution to $pp \to pp\gamma$ using the equivalent photon-flux method. We consider the diagram of Fig. 1(a). The main contribution comes from the region where the absolute value of the invariant mass squared t_1 of the exchanged photon γ^* is very small; see Fig. 8(a). In the following we work in the overall c.m. system of the reaction (2.1) where we have

$$p_a^0 = p_b^0 = \frac{1}{2}\sqrt{s},$$
$$p_1'^0 = \frac{1}{2\sqrt{s}}(s + m_p^2 - s_2). \quad \text{(B1)}$$

With ϑ the angle between $\boldsymbol{p_1'}$ and $\boldsymbol{p_a}$ we get

$$|t_1| = 2(p_a, p_1') - 2m_p^2$$
$$= 2p_a^0 p_1'^0 - 2m_p^2 - 2|\boldsymbol{p_a}||\boldsymbol{p_1'}| \cos\vartheta, \quad \text{(B2)}$$

having the minimal value

$$|t_1|_{\min} = 2(p_a^0 p_1'^0 - m_p^2 - |\boldsymbol{p_a}||\boldsymbol{p_1'}|)$$
$$= \frac{(s_2 - m_p^2)^2 m_p^2}{2s(p_a^0 p_1'^0 - m_p^2 + |\boldsymbol{p_a}||\boldsymbol{p_1'}|)}. \quad \text{(B3)}$$

For our case we have (see Fig. 4)

$$\sqrt{s} = 13 \text{ TeV}, \qquad \sqrt{s} \gg W_2 = \sqrt{s_2} \geq 10 \text{ GeV},$$
$$|t_1|_{\min} \cong \left(\frac{W_2}{\sqrt{s}}\right)^4 m_p^2. \quad \text{(B4)}$$

Numerically we get

$$|t_1|_{\min} \cong 3.1 \times 10^{-13} \text{ GeV}^2 \quad \text{for } W_2 = 10 \text{ GeV},$$
$$|t_1|_{\min} \cong 4.9 \times 10^{-8} \text{ GeV}^2 \quad \text{for } W_2 = 200 \text{ GeV}. \quad \text{(B5)}$$

These are very small values for $|t_1|$ where the equivalent photon method should give good estimates.

The equivalent photon fluxes of various particles are listed in Appendix D of Ref. [48]. For the proton this flux reads for our case

$$dn(q_1^0, t_1) = \frac{\alpha_{\text{em}}}{\pi} \frac{dq_1^0}{q_1^0} \frac{d|t_1|}{|t_1|} \left[\left(1 - \frac{q_1^0}{p_a^0}\right) D(t_1) + \frac{1}{2}\left(\frac{q_1^0}{p_a^0}\right)^2 C(t_1) \right.$$
$$\left. - \left(1 - \frac{q_1^0}{p_a^0}\right) \frac{|t_1|_{\min}}{|t_1|} D(t_1) \right]. \quad \text{(B6)}$$

Here

$$C(t) = G_M^2(t),$$
$$D(t) = [4m_p^2 G_E^2(t) - t G_M^2(t)][4m_p^2 - 1]^{-1}, \quad \text{(B7)}$$

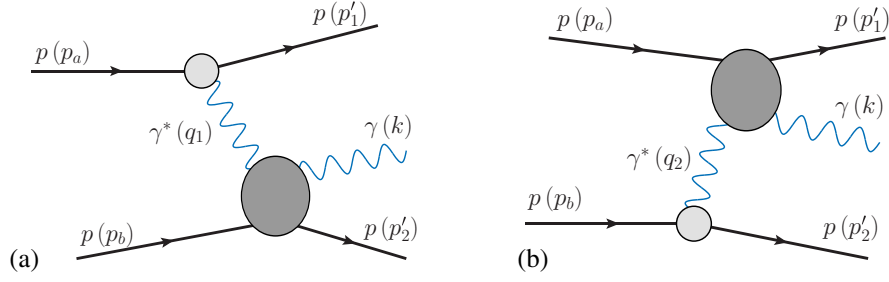and G_E and G_M are the electric and magnetic form factor of the proton, respectively,

$$G_E(t) = F_1(t) + \frac{t}{4m_p^2} F_2(t),$$
$$G_M(t) = F_1(t) + F_2(t). \quad \text{(B8)}$$

In our case we have

$$W_2^2 \cong 2q_1^0\sqrt{s},$$
$$\frac{q_1^0}{p_a^0} \cong \frac{W_2^2}{s} \ll 1,$$
$$\frac{dq_1^0}{q_1^0} = \frac{2dW_2}{W_2}. \quad \text{(B9)}$$

We can, thus, neglect in (B6) the terms with q_1^0/p_a^0 and $(q_1^0/p_a^0)^2$ and set $D(t_1) \approx 1$. We get then as an estimate for the cross section via the $\gamma\mathbb{P}$ fusion

$$d\sigma(pp \to pp\gamma)|_{\gamma\mathbb{P}\text{ fusion}}$$
$$\cong dn(q_1^0, t_1)\sigma_{\text{T}}^{\gamma p \to \gamma p}\left(t_1 = 0, W_2 = \sqrt{2q_1^0\sqrt{s}}\right)$$
$$= \frac{2\alpha_{\text{em}}}{\pi} \frac{dW_2}{W_2} \frac{d|t_1|}{|t_1|} \left(1 - \frac{|t_1|_{\min}}{|t_1|}\right) \sigma_{\text{T}}^{\gamma p \to \gamma p}(0, W_2). \quad \text{(B10)}$$

FIG. 11. General diagrams for photon production with γ^* exchange.

Here $\sigma_T^{\gamma p \to \gamma p}(0, W)$ is the total cross section for Compton scattering of a real photon on the proton at c.m. energy W. Now we integrate (B10) over $|t|$ from $|t_1|_{min}$ to a maximal value $|t_1|_{max}$ which we set to 1 GeV^2. We get then

$$\frac{d\sigma(pp \to pp\gamma)}{dW_2}\bigg|_{\gamma\mathbb{P}\text{fusion}}$$

$$\cong \frac{2\alpha_{em}}{\pi} \frac{1}{W_2} \int_{|t_1|_{min}}^{|t_1|_{max}} \frac{d|t_1|}{|t_1|}\left(1 - \frac{|t_1|_{min}}{|t_1|}\right)\sigma_T^{\gamma p \to \gamma p}(0, W_2)$$

$$\cong \frac{2\alpha_{em}}{\pi} \frac{1}{W_2}\left[\ln\frac{|t_1|_{max}}{|t_1|_{min}} - 1 + \frac{|t_1|_{min}}{|t_1|_{max}}\right]\sigma_T^{\gamma p \to \gamma p}(0, W_2). \quad (B11)$$

With $|t_1|_{max} = 1$ GeV^2 and $|t_1|_{min}$ from (B5) we get

$$\frac{2\alpha_{em}}{\pi}\left[\ln\frac{|t_1|_{max}}{|t_1|_{min}} - 1 + \frac{|t_1|_{min}}{|t_1|_{max}}\right] \cong \begin{cases} 0.13 & \text{for } W_2 = 10 \text{ GeV}, \\ 0.07 & \text{for } W_2 = 200 \text{ GeV}. \end{cases}$$

$$(B12)$$

That is, this quantity has a slow decrease with W_2.

From Fig. 3 of Ref. [40] we see that the cross section $\sigma_T^{\gamma p \to \gamma p}(0, W)$ is around 100 nb for $W \simeq 10$ GeV and slowly rising with W. Therefore, we get as an estimate

$$\frac{d\sigma(pp \to pp\gamma)}{dW_2}\bigg|_{\gamma\mathbb{P}\text{fusion}} \cong 1.3\frac{10}{W_2} \text{ nb/GeV}. \quad (B13)$$

Here W_2 has to be included in GeV. Our estimate gives a cross section falling roughly as $1/W_2$ with a size of order 0.3 nb/GeV for $W_2 = 40$ GeV.

We can compare this with the result of the explicit calculation shown in the right panel of Fig. 3. Since here W_1 is plotted we must compare with the dashed red line corresponding to the $\mathbb{P}/\mathbb{R}\gamma$ fusion. And, indeed, this cross section is not far from 0.3 nb/GeV for $W_1 = 40$ GeV and it is falling with increasing W_1 according to a $1/W_1$ law.

APPENDIX C: CEP OF PHOTONS IN THE LIMIT $k \to 0$

In this appendix we investigate the CEP mechanism for photons in the limit that the four momentum k of the photon approaches zero. We know from Low's theorem [7] that in

this limit the bremsstrahlungs mechanism will dominate. But we find it interesting to see how CEP goes over to bremsstrahlung for $k \to 0$.

Let us start with the diagrams with γ^* exchange shown in Fig. 1. For general W_1 and W_2 we write them as emission of γ^* followed by the scattering process $\gamma^* p \to \gamma p$ as shown in Fig. 11.

For $k \to 0$ we have from (2.2) $W_1^2, W_2^2 \to m_p^2$ and the description of the $\gamma^* p \to \gamma p$ scattering by t-channel exchanges as shown in Fig. 1 will certainly no longer be adequate. We note that for real Compton scattering on an electron

$$\gamma(q) + e(p) \to \gamma(k) + e(p'), \quad (C1)$$

with the initial and final photons on shell, there exists a low energy theorem in QED proven by Thirring [49]. In the limit $k \to 0$ the amplitude for (C1) is given exactly by the s and u channel diagrams shown in Fig. 12.

Thus, we expect that also in our case where we have in Figs. 11(a) and 11(b)

$$\gamma^*(q_1) + p(p_b) \to \gamma(k) + p(p_2') \quad (C2)$$

and

$$\gamma^*(q_2) + p(p_a) \to \gamma(k) + p(p_1'), \quad (C3)$$

respectively, the analogous s and u channel diagrams will be important. Inserting these in the diagrams of Figs. 11(a) and 11(b) we get the diagrams of Fig. 13 which are exactly the bremsstrahlung diagrams associated with the basic γ^* exchange. We know from Low's theorem [7] that for $k \to 0$ these diagrams give the leading behavior proportional to $1/\omega$ in the $pp \to pp\gamma$ amplitude when the basic diagram
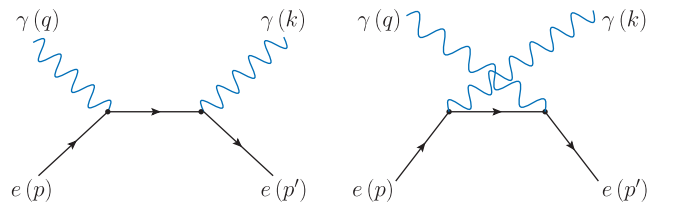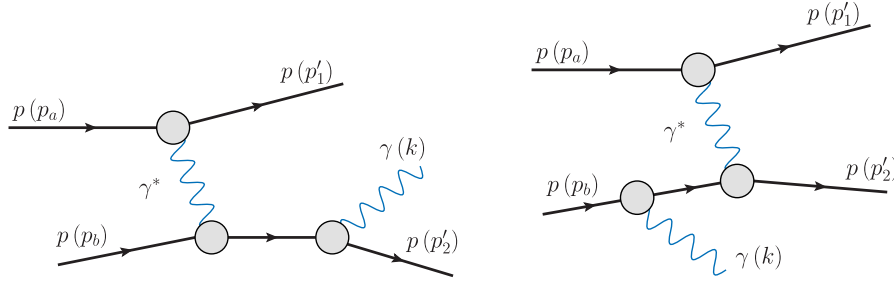

FIG. 12. The s and u channel diagrams for $\gamma e \to \gamma e$.

FIG. 13. Bremsstrahlungs diagrams obtained from the diagram Fig. 11(a) for $k \to 0$. From the diagram Fig. 11(b) we get for $k \to 0$ the analogous diagrams where the final photon $\gamma(k)$ is emitted from the upper proton line.

for $pp \to pp$ is the one with γ^* exchange. That is, for $k \to 0$ the diagrams of Fig. 11 give those of the QED bremsstrahlung process; see Table I.

To summarize: for high W_1 and W_2, greater than 6 GeV say, the most important contributions to $\gamma^* p \to \gamma p$ in the diagrams of Fig. 11 will come from the t-channel exchanges, $\mathbb{P} + \mathbb{R}_+$. This then leads to the $\gamma - \mathbb{P}/\mathbb{R}$ CEP process. For $W_{1,2} \to m_p^2$, on the other hand, the diagrams of Fig. 11 give the QED bremsstrahlung ones. For intermediate values of $W_{1,2}$ a simple addition of contributions from s, u, and t channel diagrams for $\gamma^* p \to \gamma p$ is probably not the right thing to do. We have to recall the duality arguments which were initiated by

the discovery of the Veneziano amplitude [50]. We think that, therefore, a strict separation of CEP and bremsstrahlungs-type contributions to $pp \to pp\gamma$ is in general not possible.

The $k \to 0$ behavior of the amplitudes of the diffractive contributions to photon CEP, see Sec. II B and Fig. 2, can be discussed in an analogous way. For $k \to 0$ we shall obtain from the analogs of Fig. 11 with γ^* replaced by hadronic exchanges the diffractive bremsstrahlungs diagrams for $pp \to pp\gamma$ shown in Figs. 3(a)–3(f) of Ref. [2]. There only $\mathbb{P}$ exchange is shown but its replacement by the other hadronic exchanges, $f_{2\mathbb{R}}$, $a_{2\mathbb{R}}$, $\mathbb{O}$, $\omega_\mathbb{R}$, $\rho_\mathbb{R}$, is mentioned in the figure caption.

[1] P. Lebiedowicz, O. Nachtmann, and A. Szczurek, High-energy $\pi\pi$ scattering without and with photon radiation, Phys. Rev. D **105**, 014022 (2022).

[2] P. Lebiedowicz, O. Nachtmann, and A. Szczurek, Soft-photon radiation in high-energy proton-proton collisions within the tensor-Pomeron approach: Bremsstrahlung, Phys. Rev. D **106**, 034023 (2022).

[3] D. Adamová et al., A next-generation LHC heavy-ion experiment, arXiv:1902.01211 [physics.ins-det].

[4] P. Braun-Munzinger, Experimental opportunities for new physics at low transverse momentum, in *A lecture given at the XXIXth International Conference on Ultra-relativistic Nucleus-Nucleus Collisions* (Kraków, Poland, 2022) https://qm2021.syskonf.pl.

[5] *Workshop EMMI Rapid Reaction Task Force on "Real and virtual photon production at ultra-low transverse momentum and low mass at LHC"*, organized by K. Schweda, R. Bailhache, and S. Flörchinger, https://indico.gsi.de/event/11529/overview.

[6] ALICE Collaboration, Letter of intent for ALICE 3: A next-generation heavy-ion experiment at the LHC, Report No. CERN-LHCC-2022-009, LHCC-I-038, arXiv:2211.02491 [physics.ins-det].

[7] F. E. Low, Bremsstrahlung of very low-energy quanta in elementary particle collisions, Phys. Rev. **110**, 974 (1958).

[8] A. T. Goshaw, J. R. Elliott, L. E. Evans, L. R. Fortney, P. W. Lucas, W. J. Robertson, W. D. Walker, I. J. Kim, and C.-R. Sun, Direct Photon Production from $\pi^+ p$ Interactions at 10.5 GeV/c, Phys. Rev. Lett. **43**, 1065 (1979).

[9] P. V. Chliapnikov, E. A. De Wolf, A. B. Fenyuk, L. N. Gerdyukov, Y. Goldschmidt-Clermont, V. M. Ronzhin, and A. Weigend (Brussels-CERN-Genoa-Mons-Nijmegen-Serpukhov Collaboration), Observation of direct soft photon production in $K^+ p$ interactions at 70 GeV/c, Phys. Lett. **141B**, 276 (1984).

[10] F. Botterweck et al. (EHS/NA22 Collaboration), Direct soft photon production in $K^+ p$ and $\pi^+ p$ interactions at 250 GeV/c, Z. Phys. C **51**, 541 (1991).

[11] S. Banerjee et al. (SOPHIE/WA83 Collaboration), Observation of direct soft photon production in $\pi^- p$ interactions at 280 GeV/c, Phys. Lett. B **305**, 182 (1993).

[12] J. Antos et al., Soft photon production in 400 GeV/c p-Be collisions, Z. Phys. C **59**, 547 (1993).

[13] M. L. Tincknell et al., Low transverse momentum photon production in proton-nucleus collisions at 18 GeV/c, Phys. Rev. C **54**, 1918 (1996).

[14] A. Belogianni et al. (WA91 Collaboration), Confirmation of a soft photon signal in excess of Q.E.D. expectations in $\pi^- p$ interactions at 280 GeV/c, Phys. Lett. B **408**, 487 (1997).

[15] A. Belogianni *et al.*, Further analysis of a direct soft photon excess in $\pi^- p$ interactions at 280 GeV/c, Phys. Lett. B **548,** 122 (2002).

[16] A. Belogianni *et al.*, Observation of a soft photon signal in excess of QED expectations in pp interactions, Phys. Lett. B **548,** 129 (2002).

[17] J. Abdallah *et al.* (DELPHI Collaboration), Evidence for an excess of soft photons in hadronic decays of Z^0, Eur. Phys. J. C **47,** 273 (2006).

[18] J. Abdallah *et al.* (DELPHI Collaboration), Observation of the muon inner bremsstrahlung at LEP1, Eur. Phys. J. C **57,** 499 (2008).

[19] J. Abdallah *et al.* (DELPHI Collaboration), Study of the dependence of direct soft photon production on the jet characteristics in hadronic Z^0 decays, Eur. Phys. J. C **67,** 343 (2010).

[20] C.-Y. Wong, An overview of the anomalous soft photons in hadron production, Proc. Sci. Photon2013 (**2014**) 002 [arXiv:1404.0040].

[21] G. W. Botz, P. Haberl, and O. Nachtmann, Soft photons in hadron-hadron collisions: synchrotron radiation from the QCD vacuum?, Z. Phys. C **67,** 143 (1995).

[22] O. Nachtmann, Spin correlations in the Drell-Yan process, parton entanglement, and other unconventional QCD effects, Ann. Phys. (Amsterdam) **350,** 347 (2014).

[23] C. Ewerz, M. Maniatis, and O. Nachtmann, A model for soft high-energy scattering: Tensor Pomeron and vector Odderon, Ann. Phys. (Amsterdam) **342,** 31 (2014).

[24] C. Ewerz, P. Lebiedowicz, O. Nachtmann, and A. Szczurek, Helicity in proton-proton elastic scattering and the spin structure of the Pomeron, Phys. Lett. B **763,** 382 (2016).

[25] L. Adamczyk *et al.* (STAR Collaboration), Single spin asymmetry A_N in polarized proton-proton elastic scattering at $\sqrt{s} = 200$ GeV, Phys. Lett. B **719,** 62 (2013).

[26] D. Britzger, C. Ewerz, S. Glazov, O. Nachtmann, and S. Schmitt, Tensor Pomeron and low-x deep inelastic scattering, Phys. Rev. D **100,** 114007 (2019).

[27] A. Bolz, C. Ewerz, M. Maniatis, O. Nachtmann, M. Sauter, and A. Schöning, Photoproduction of $\pi^+\pi^-$ pairs in a model with tensor-Pomeron and vector-Odderon exchange, J. High Energy Phys. 01 (2015) 151.

[28] P. Lebiedowicz, O. Nachtmann, and A. Szczurek, Exclusive central diffractive production of scalar and pseudoscalar mesons; tensorial vs. vectorial Pomeron, Ann. Phys. (Amsterdam) **344,** 301 (2014).

[29] P. Lebiedowicz, O. Nachtmann, and A. Szczurek, ρ^0 and Drell-Söding contributions to central exclusive production of $\pi^+\pi^-$ pairs in proton-proton collisions at high energies, Phys. Rev. D **91,** 074023 (2015).

[30] P. Lebiedowicz, O. Nachtmann, and A. Szczurek, Central exclusive diffractive production of the $\pi^+\pi^-$ continuum, scalar, and tensor resonances in pp and $p\bar{p}$ scattering within the tensor Pomeron approach, Phys. Rev. D **93,** 054015 (2016).

[31] P. Lebiedowicz, O. Nachtmann, and A. Szczurek, Central production of ρ^0 in pp collisions with single proton diffractive dissociation at the LHC, Phys. Rev. D **95,** 034036 (2017).

[32] P. Lebiedowicz, O. Nachtmann, and A. Szczurek, Exclusive diffractive production of $\pi^+\pi^-\pi^+\pi^-$ via the intermediate $\sigma\sigma$ and $\rho\rho$ states in proton-proton collisions within tensor Pomeron approach, Phys. Rev. D **94,** 034017 (2016).

[33] P. Lebiedowicz, O. Nachtmann, and A. Szczurek, Central exclusive diffractive production of $p\bar{p}$ pairs in proton-proton collisions at high energies, Phys. Rev. D **97,** 094027 (2018).

[34] P. Lebiedowicz, O. Nachtmann, and A. Szczurek, Towards a complete study of central exclusive production of K^+K^- pairs in proton-proton collisions within the tensor Pomeron approach, Phys. Rev. D **98,** 014001 (2018).

[35] P. Lebiedowicz, O. Nachtmann, and A. Szczurek, Searching for the Odderon in $pp \to ppK^+K^-$ and $pp \to pp\mu^+\mu^-$ reactions in the $\phi(1020)$ resonance region at the LHC, Phys. Rev. D **101,** 094012 (2020).

[36] P. Lebiedowicz, O. Nachtmann, and A. Szczurek, Central exclusive diffractive production of $K^+K^-K^+K^-$ via the intermediate $\phi\phi$ state in proton-proton collisions, Phys. Rev. D **99,** 094034 (2019).

[37] P. Lebiedowicz, O. Nachtmann, and A. Szczurek, Extracting the Pomeron-Pomeron-$f_2(1270)$ coupling in the $pp \to pp\pi^+\pi^-$ reaction through the angular distribution of the pions, Phys. Rev. D **101,** 034008 (2020).

[38] P. Lebiedowicz, J. Leutgeb, O. Nachtmann, A. Rebhan, and A. Szczurek, Central exclusive diffractive production of axial-vector $f_1(1285)$ and $f_1(1420)$ mesons in proton-proton collisions, Phys. Rev. D **102,** 114003 (2020).

[39] P. Lebiedowicz, Study of the exclusive reaction $pp \to ppK^{*0}\bar{K}^{*0}$: $f_2(1950)$ resonance versus diffractive continuum, Phys. Rev. D **103,** 054039 (2021).

[40] P. Lebiedowicz, O. Nachtmann, and A. Szczurek, Deeply virtual Compton scattering in the tensor-Pomeron approach, Phys. Lett. B **835,** 137497 (2022).

[41] P. Lebiedowicz and A. Szczurek, Exclusive diffractive photon bremsstrahlung at the LHC, Phys. Rev. D **87,** 114013 (2013).

[42] J. Breitweg *et al.* (ZEUS Collaboration), Elastic and proton-dissociative ρ^0 photoproduction at HERA, Eur. Phys. J. C **2,** 247 (1998).

[43] V. Andreev *et al.* (H1 Collaboration), Measurement of exclusive $\pi^+\pi^-$ and ρ^0 meson photoproduction at HERA, Eur. Phys. J. C **80,** 1189 (2020).

[44] G. Antchev *et al.* (TOTEM Collaboration), First determination of the ρ parameter at $\sqrt{s} = 13$ TeV: Probing the existence of a colourless C-odd three-gluon compound state, Eur. Phys. J. C **79,** 785 (2019).

[45] ATLAS Collaboration, Measurement of the total cross section and ρ-parameter from elastic scattering in pp collisions at $\sqrt{s} = 13$ TeV with the ATLAS detector, Report No. CERN-EP-2022-129, arXiv:2207.12246 [hep-ex].

[46] G. Antchev *et al.* (TOTEM Collaboration), Elastic differential cross-section measurement at $\sqrt{s} = 13$ TeV by TOTEM, Eur. Phys. J. C **79,** 861 (2019).

[47] A. Donnachie, H. G. Dosch, P. V. Landshoff, and O. Nachtmann, Pomeron physics and QCD, Cambridge Monogr. Part. Phys., Nucl. Phys., Cosmol. **19,** 1 (2002).

[48] V. M. Budnev, I. F. Ginzburg, G. V. Meledin, and V. G. Serbo, The two-photon particle production mechanism. Physical problems. Applications. Equivalent photon approximation, Phys. Rep. **15,** 181 (1975).

[49] W. E. Thirring, Radiative corrections in the nonrelativistic limit, Philos. Mag. **41,** 1193 (1950).

[50] G. Veneziano, Construction of a crossing—symmetric, Regge behaved amplitude for linearly rising trajectories, Nuovo Cimento A **57,** 190 (1968).